INVESTIGATION OF ENHANCED-REFLECTIVITY FEATURES EMBEDDED WITHIN A WINTERTIME OROGRAPHIC CLOUD ON 28-29 NOVEMBER 1984

submitted by

Ian T. Baker

Department of Atmospheric Science

In partial fulfullment of the requirements
for the Degree of Master of Science
Colorado State University
Fort Collins, Colorado
Fall, 1994

COLORADO STATE UNIVERSITY

28 October, 1994

WE HEREBY RECOMMEND THAT THE THESIS PREPARED UNDER OUR SUPERVISION BY IAN T. BAKER ENTITLED INVESTIGATION OF ENHANCED-REFLECTIVITY FEATURES EMBEDDED WITHIN A WINTERTIME OROGRAPHIC CLOUD ON 28-29 NOVEMBER 1984 BE ACCEPTED AS FULFILLING IN PART REQUIREMENTS FOR THE DEGREE OF MASTER OF SCIENCE.

Committee on Graduate Work

Paul W. Mielke

William R. Cotton

Lewis O. Grant
Adviser

Stephen K. Cox
Department Head

Abstract

INVESTIGATION OF ENHANCED-REFLECTIVITY FEATURES EMBEDDED WITHIN A WINTERTIME OROGRAPHIC CLOUD ON 28-29 NOVEMBER 1984

A combination of aircraft, sounding, surface, vertically-pointing ku-Band radar and dual-channel radiometer data was used to investigate the microphysical characteristics of enhanced-reflectivity areas embedded within an orographic cloud in northwestern Colorado on 28-29 November 1984. The orographic cloud was associated with the passage of an open wave and upper-level front over the region, and embedded within the cloud were regularly-spaced areas of increased reflectivity as seen by the vertically-pointing radar. The radiometer observed a cyclical component on both the liquid and vapor channels when oriented in the vertical. Aircraft data reveal that there was supercooled liquid water in the cloud at levels as high as 41 kPa and as far as 55 km upwind of the barrier. 2D-C and 2D-P probe data indicated two crystal regimes, one where concentrations in individual size bins were larger and spectra were broader, indicating crystal growth. In the other, concentrations were smaller and size spectra were narrower. Radar data indicate that the enhanced-reflectivity regions were between 10-20 km apart, with a length dimension on the order of 5 km wide. It is believed that the presence of the enhanced-reflectivity areas is closely linked to the presence of a decoupled layer on the windward side of the barrier, and preliminary evidence points to a gravity-wave mechanism as a physical cause.

Ian T. Baker
Department of Atmospheric Science
Colorado State University
Fort Collins, CO 80523
Fall 1994

ACKNOWLEDGEMENTS

The creation of this document has been an arduous process, during which I learned as much about myself as I did about orographic clouds. The complete list of those who have supported me, advisors, family and friends, is much too long to list here. However, there are certain individuals who stand out and, as such, merit recognition.

I would like to thank my advisor, Professor Lewis O. Grant, and my advising committee, Drs. William Cotton and Paul Mielke. Drs. David C. Rogers and Paul J. Demott, while not on my committee, were vital for day-to-day assistance, and their patience and help has been invaluable. Ian Wittmeyer, Ben Bernstein, Doug Wesley, Marcia Politovich, Roy Rasmussen, Peter Neilley, Teddy Keller, Mark Branson and Kelley Wittmeyer all took the time to assist in various aspects of the research.

This paper is dedicated to the memory of John Kozlowsky and Antoinette Gerdus.

Table of Contents

List of Figures

1. INTRODUCTION

The distribution of supercooled liquid water (SLW), ice, and water vapor in wintertime orographic clouds has been investigated, usually from a weather modification standpoint, by field projects in California (Sierra Cooperative Pilot Project–SCCP), Colorado (Colorado Orographic Seeding Experiments–COSE I-IV), and the Tushar Mountains of Utah. The present study utilizes data from the fourth COSE project (COSE IV), which was conducted in the winter of 1984-85 for further investigation into these distributions. A combination of remote sensors, surface, sounding and aircraft data were used to examine small-scale variations in the temporal evolution of the water field in all phases within the orographic cloud. The temporal evolution of SLW, vapor and ice was seen to have a variable component, and the nature of these relatively high-frequency features are described. The instrument suite was such that description of the spatial characteristics of the water field in three dimensions was difficult. Where possible, however, such a description was obtained and the implied spatial and temporal characteristics of the water field was described in terms of conceptual models put forth by others.

Data from 28-29 November 1984 were analyzed, with emphasis on transient regions of enhanced reflectivity that were seen to pass over a stationary, vertically-pointing radar. The suggestion is that these features were banded in nature, with a coherent structure pertaining to their frequency and microphysical characteristics. The enhanced-reflectivity features can be seen to be positively correlated with periods of enhanced snowfall accumulation, and can be seen to possess higher concentrations of SLW, ice particles, and precipitation-sized particles at most levels within the cloud.

Several possible generation mechanisms were investigated in an effort to develop a conceptual model of the dynamics of the orographic cloud with respect to these enhanced-reflectivity features. It will be seen that the development and propagation of these enhanced-reflectivity features were closely linked to the presence of a blocked or decoupled layer upwind of the barrier. It is suggested that once formed, these features move with the winds above the decoupled layer and were advected into the region of heavy cloud associated with the region of maximum orographic lift near the barrier. A relationship between these enhanced-reflectivity features and snowfall accumulation upwind of the region normally associated with maximum orographic snowfall is hypothesized.

In the following sections a single case from the COSE IV dataset will be examined with the emphasis on describing these bands or cells of enhanced activity embedded within the cloud. Remote sensing, aircraft and surface data were analyzed in an attempt to describe the temporal and spatial evolution of the vapor, liquid and ice fields within a single orographic cloud. The main points to be drawn from this case study are as follows:

- There existed a layer upwind of the barrier which was decoupled from the mean flow
- Vertically pointing Ku-band radar noted periodic enhanced-reflectivity features, estimated to be 10 to 20 km apart and 5 to 30 km wide
- Aircraft data revealed the presence of two distinct microphysical regimes, one where size spectra are narrow and numbers are small, another where size spectra are wider and numbers larger
- Vertically pointing radiometer data indicate a periodicity in the path-integrated SLW and vapor depths

- Spectral analysis indicates a period of near 30 minutes for SLW and derived path-integrated ice depth
- Preliminary results suggest the periodicity is caused by a gravity wave that sets up along the interface between the decoupled layer and the mean flow

The single case studied, while characteristic of wintertime orographic storms in the region, cannot be assumed to represent all storms in the area.

2. BACKGROUND

2.1 COLORADO OROGRAPHIC SEEDING EXPERIMENTS

Sassen (1984) used a remote sensor approach to investigate the temporal evolution of the combined water field from a prefrontal storm event from COSE III. His primary instrument was a ruby lidar, which was utilized in conjuction with dual wavelength microwave radiometer and vertically-pointing Ku-band radar data. The lidar made possible findings about the spatial and temporal nature of liquid layers within a deep orographic cloud which were not possible with path-integrated radiometric data. For the case that Sassen studied (18 January 1982), it was determined that liquid water was found in approximately 0.5 km deep layers, with temperatures generally at or near -30, -24, and -17 degrees C. These three layers were found to decrease in height as the storm center approached. It was also noted that there was an inverse relationship between liquid and ice amounts in the cloud, but that vapor and liquid are positively related. Aggregation was determined, through the use of lidar data, to be constrained to very thin layers within the cloud. Finally, Sassen noted that the total water (vapor+liquid+ice) amount was not a constant value, but fluctuated in irregular cycles.

The spatial and temporal characteristics of cloud water in cloud systems over northwestern Colorado in the COSE domain were investigated by Rauber *et al.* (1986) and Rauber and Grant (1986). These cloud systems were defined as prefrontal, frontal and postfrontal, as well as orographic (not associated with a major cyclonic event). Liquid water was detected in almost all stages of these storms, with the highest liquid water contents found prior to the onset of precipitation. All storm systems were found to have very low droplet concentrations, generally <300 cm^{-3}, and quite commonly <100 cm^{-3}. In the latter case, broad droplet size distributions were observed, with significant numbers of droplets $> 20\mu$m in size. Liquid water production was described as occurring in 'zones' or areas of vertical motion induced by either gravity waves induced by topography, or vertical motion generated by convective or shear instability. Liquid water was found to occur in three zones of the cloud, namely cloud base, cloud top, and regions of maximum orographic lift near the barrier. An inverse relationship between liquid water content and precipitation was found, which is consistent with Sassen's findings. Conceptual models of the spatial distribution of SLW in three different Park Range cloud systems were developed, and are shown in Figure 1.

Rauber (1987) compiled a climatology of 17 winter storms from the COSE III dataset, describing cloud, ice and precipitation processes. Cloud top and regions of strong orographic forcing were found to be primary regions of ice production, with fragmentation the main secondary form of ice particle production. It was concluded that Hallet-Mossop and droplet fragmentation during freezing were not significant forms of ice multiplication, due to the lack of large droplets in the cloud. Surface precipitation was dominated by dendritic snowfall, which requires water saturation in the region between $-13°$ and $-17°$C. Many snow crystals formed at temperatures colder than $-20°$C, and crystal trajectories were found to begin far upwind.

In another study from COSE III, Uttal *et al.* (1988) used data taken from aircraft penetrations to construct a spatial view of liquid, vapor and ice fields in a stable orographic cloud. Flight restrictions prevented collection of data at altitudes below about 4 km msl, and conditions had to be considered static in order to circumvent the fact that the aircraft could not sample more than one region of the cloud at a given time. This quasi-stationary assumption enabled Uttal to describe the water fields for the given case as constant in space and time as a function of topography. The results show that the concentrations of liquid, vapor and ice all decreased quickly

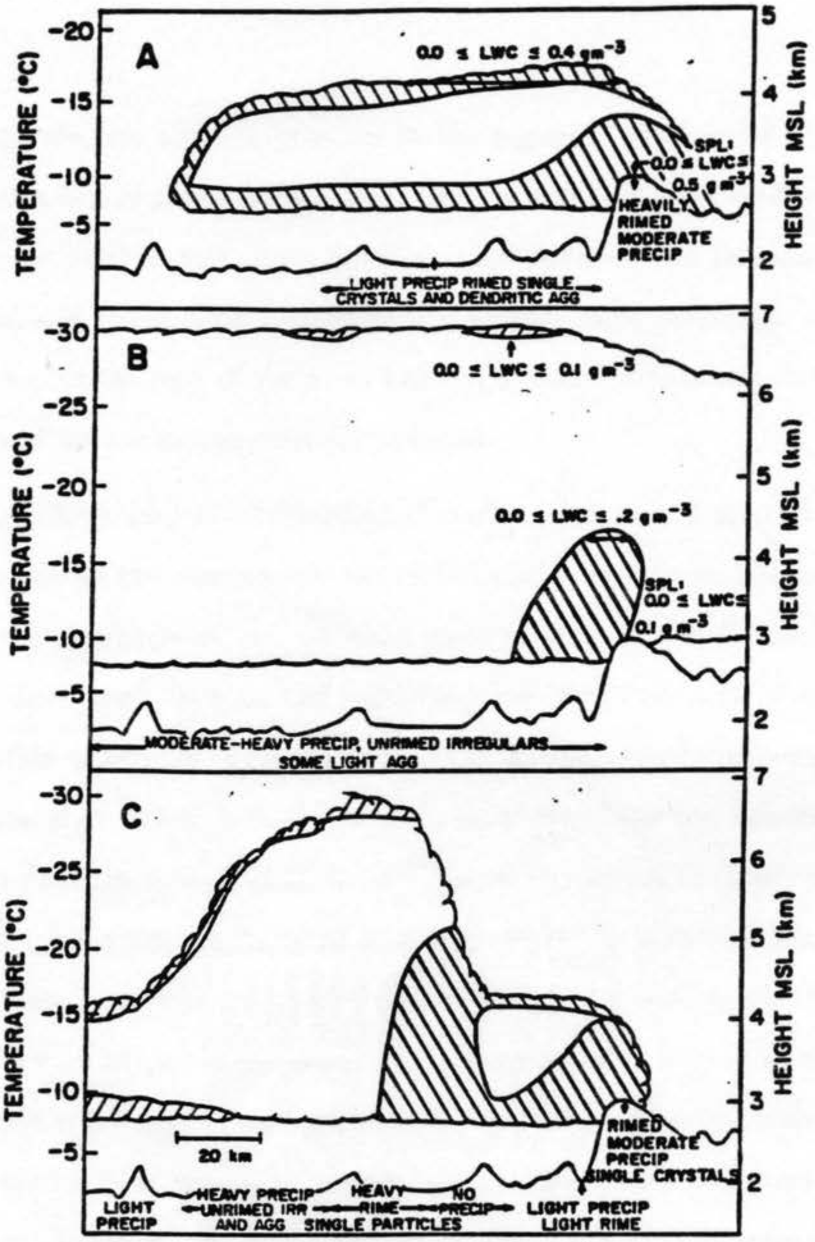

Figure 1: Conceptual models of supercooled liquid water distribution in Park Range cloud systems for (A) a shallow stratiform cloud system with a warm cloud top temperature (CTT > −22°C; (B) a deep stratiform system with a cold cloud top temperature; and (C) a deep convective region embedded in a shallow stratiform system. The characteristic precipitation type is listed for each case along the bottom of the figure. Magnitudes of liquid water contents measured with aircraft or at surface stations are shown on the figure. (from Rauber and Grant, 1986)

above the minimum aircraft altitude of 4 km in the region of the barrier. Vapor density decreased at a rate of about 0.5 gm^{-3} per 1000 m, and liquid and ice decrease to negligible values by 6000 m msl. Both liquid and ice densities had maxima over the barrier. Liquid and vapor both also showed a smaller local maximum over a smaller barrier 30 km to the west of the main barrier, and the implication was that maxima of liquid and ice are topographically induced.

Peterson *et al.* (1991) used a combination of surface station and aircraft data from COSE III, as well as two-dimensional numerical simulations to investigate the decoupling of low-level flow from the synoptic scale winds. Figure 2 shows the conceptual model developed, wherein the decoupled low-level flow acts to extend the orographic surface upwind, so that orographic lift is experienced upwind of the actual barrier. It was shown that in cases where the decoupled layer was nonexistent or extended a short distance upwind of the barrier, parcel rise tended to closely follow the topography. In cases where the decoupled layer extended far upstream from the barrier, parcel rise bore little or no resemblance to the underlying topography. When the area of initial parcel lift is shifted upstream, precipitation is shifted upstream as well. Precipitation efficiency is increased as well, presumably because condensate production is initiated further upstream, giving ice crystals a longer trajectory (and longer growth times) in which to grow in the area of orographic lift upstream of the barrier.

2.2 COLORADO RIVER BASIN PILOT PROJECT

Five years of investigation of storms in the San Juan Mountains of southwestern Colorado were summarized by Marwitz (1980) and Cooper and Saunders (1980). Most storms were found to follow a sequence of four stages: stable, neutral, unsta-

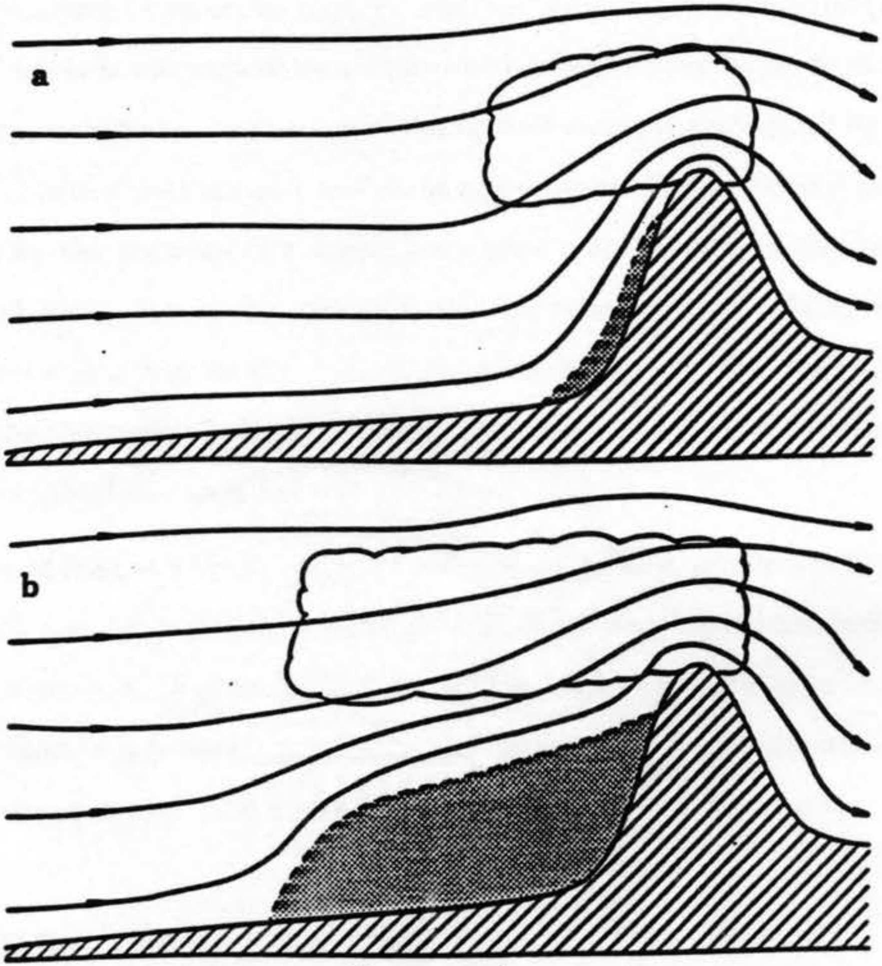

Figure 2: Conceptual model of the hypothesis that low-level decoupled flow (stippled area) acts as an extension of the mountain barrier for orographic lift purposes which would then alter the location of condensate production and hence precipitation. A small amount of decoupled low-level flow (a) allows parcel lift to occur near the barrier while a large amount of low-level decoupled flow (b) forces parcel lift to occur upstream of the barrier. (from Peterson *et al.*, 1991)

ble, and dissipation. The stable stage was distinguished by blocked or decoupled flow near the windward base of the barrier, such that winds below mountaintop level were diverted towards the west or away from the barrier. As the upper level baroclinic zone approached the storm entered the neutral stage, characterized by deep cloud, typically extending through much of the troposphere. The unstable stage was characterized by the presence of a convergence zone near the base of the barrier, and embedded convection in the cloud. It was hypothesized that cold advection aloft starts convection high in the cloud that builds downwards, eventually acting to evacuate the thermodynamically stable air from the blocked layer. Dissipation occurred when subsidence aloft began.

During one of the cases, a near-neutral to weakly unstable θ_e profile was found at midlevels, with a stable layer aloft. Analysis of flights through this layer indicated a series of gravity waves (Figure 3) which were interpreted to be located at the base of the stable layer, and induced by wind shear. The wavelength of these waves was found to be around 4 km, which corresponds to a period of 300-400 seconds.

2.3 SIERRA COOPERATIVE PILOT PROJECT

Heggli *et al.* (1983) used data from aircraft and radar to investigate the SLW and ice crystal distributions in Sierra Nevada winter storms. The data were stratified into three precipitation echo types: area-wide, banded, and cellular. Area-wide clouds were defined as those filling the sky with few breaks, although cloud-free layers may exist. Banded echo types often consisted of a vigorous convective band with clear sky before and after, while cellular echo types consisted of scattered cells. Liquid water content/ice crystal concentration (LWC/ICC) ratios were investigated for each of the three precipitation echo types, since in a cloud seeding situation

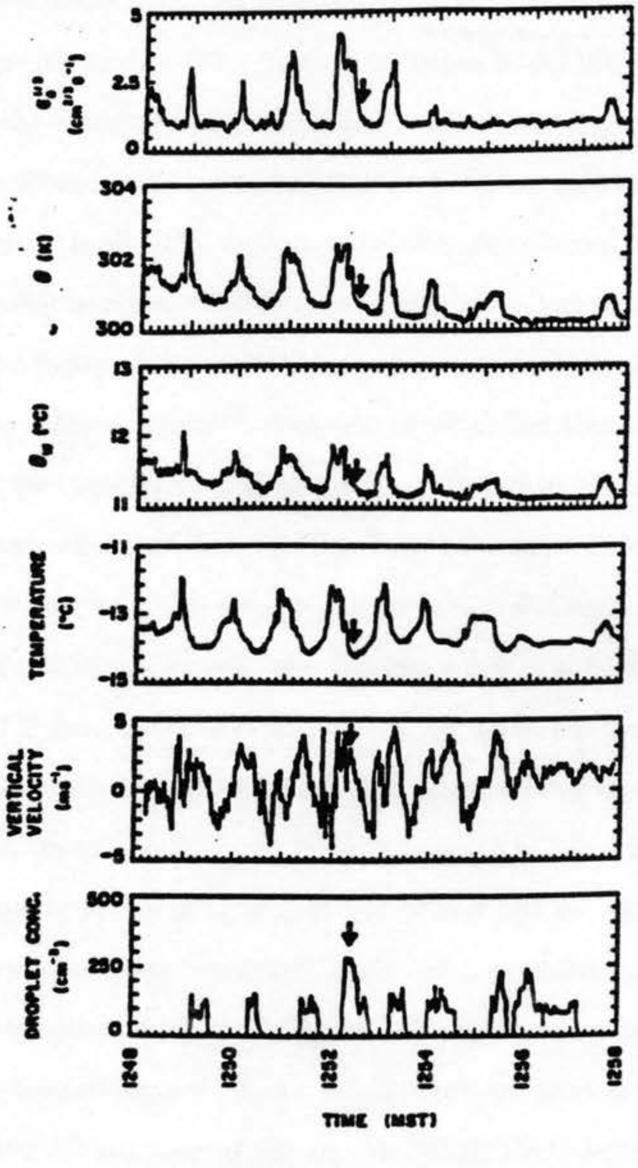

Figure 3: Analog traces of eddy dissipation rates ($\epsilon_0^{1/3}$), potential temperature (θ), wet-bulb potential temperature (θ_w), temperature, vertical velocity and droplet concentrations during a portion of the flight of 22 March 1975. The arrow near 1252.5 is a reference mark. (From Marwitz 1980)

higher LWC and lower ICC are each seen as being favorable conditions. Area-wide and banded echo types were both characterized by LWC usually below 0.25 g m^{-3} and narrow ICC from 10 to 100 L^{-1}. Both echo types had LWC/ICC ratios near 100 μg $crystal^{-1}$ at the freezing level, decreasing with decreasing temperature to a ratio near 10. The cellular echo types had higher LWC at all levels, approaching 0.5 gm^{-3} at the freezing level. ICC were more widely distributed, between 0.1 and 1000 L^{-1}, with a greater occurrence of low ICC, which was not seen nearly as often in the other two echo types. LWC/ICC ratios were more widely distributed, with some ratios as high as 100 μg $crystal^{-1}$ observed. Spatial distributions of LWC, ICC and LWC/ICC were presented in vertical cross sections through the barrier crest, with emphasis on areas of high LWC and low ICC, or areas where LWC/ICC was high. For area-wide echo types, the only areas with high LWC were near the freezing level, in areas of pronounced orographic lift. ICC were found to be low only near the freezing level, with ICC increasing with altitude in the cloud and nearer the barrier. Several pockets of LWC/ICC$>$ 0.5 occurred near the freezing level 40 to 120 km upwind of the barrier. Banded echo types revealed higher LWC, again with greatest LWC near the freezing level. Maxima were found 50 and 120 km west of the barrier. ICC were found to be similar to area-wide cases, with greatest probability of low ICC in the warmer regions of the cloud. LWC/ICC ratios were greatest in the areas of high LWC in the lowest regions of the cloud, with an area of high LWC/ICC extending up to $-15°$C 50 km west of the barrier. High LWC were found from the area of cloud formation 100 km west of the crest to 20 km west of the barrier in the cellular echo types. Low ICC were found in the areas where LWC was the greatest. LWC/ICC ratios were maximized in the region from 50-100 km west of the barrier, at temperatures $> -15°$C, with a secondary maximum directly over the barrier. In all echo types, the greatest LWC was found near the freezing level.

A method to predict increases in SLW within Sierra Nevada winter clouds after upper jet passage was developed by Reynolds and Kuciauskas (1988), where, by using a case study approach they postulate that the onset of increased SLW within the cloud can be identified prior to the event. Citing data from several case studies, the authors addressed questions pertaining to mesoscale characteristics and SLW excess in midlatitude synoptic scale storm systems and the identifiable features of these systems. It was found that in the three cases presented, the bulk of the precipitation was produced by seeder-feeder mechanisms during warm frontal overrunning, while precipitation associated with frontal passage was intense but short-lived. The passage of an upper level front and associated jet streak was found to induce rainbands followed by a lowering of cloudtop and decreasing precipitation. Reynolds and Kuciauskas specified three temporal regions of Sierra Nevada storms where excess SLW would be produced. The first exists prior to precipitation, when low-level moisture is advected over the barrier or a pre-existing stable layer at the beginning of an event. The next is behind the passage of an upper-level cold surge or humidity front, where generation of ice crystals aloft is temporarily reduced, interrupting the seeder-feeder process. Drying aloft can increase the potential instability, making increased embedded convection possible. The last temporal region containing excess SLW is in the subsident region behind the cold front. Here again upper level cloudiness and ice crystals are reduced, resulting in a reduction in the seeder-feeder process. Forced ascent of air parcels over the Sierra Nevada can result in release of potential instability manifest as embedded convection within the orographic cloud.

2.4 UTAH

Using a two-part approach, Long *et al.* (1990) and Sassen *et al.* (1990) described a complex storm from the Tushar Mountains of Utah, using an extensive array of remote sensors to evaluate the storm both on the synoptic and mesoscale level. Mesoscale kinematic fields were derived from Doppler radar data, while mesoscale structure was derived from radiometric, lidar, and Ku-band Doppler radar data. Long *et al.* subdivided a longwave trough and associated cold front passage into four segments. The first segment was comprised of nonprecipitating altostratus clouds that developed on the leading edge of the approaching longwave trough. Segment two was defined as the period during which the humidity front/cold surge passed through the area in connection with the trough. Cloud cover changed from altostratus to altocumulus due to advection of drier air over the cloudy layer, with attendant drop in θ_e at upper levels, resulting in development of convective instability. The kinematics during this second stage consisted of an increase in the low-level relative humidity due to cooling, veering of the winds to a position more orthogonal to the barrier, and an increase in windspeed. This resulted in the development of an area of convergence at low levels, with divergence aloft. Some updrafts were noted at this time. The third segment was dominated by the passage of a surface cold front, with subsequent development of a stable dome of cold air over the area. Behind the cold front, the area of convergence extended upwards and maximum values of convergence were observed. Additionally, maximum values of divergence were noted at upper levels. The maximum precipitation of the event occurred during the four hours surrounding surface frontal passage. The greatest water release rates were noted in midlevels of the cloud during the third stage, where water release at a given altitude and time is given by $C(z,t) = -w(z,t)\rho(z,t)\frac{\partial m_s(z,t)}{\partial z}$ where w is the mesoscale updraft velocity, ρ is the density of dry air, and m_s is the saturation mixing ratio with respect to ice. The fourth segment was the dissipation stage. All levels of the atmosphere became convectively stable, as a ridge approached from the west and convergence decreased.

Long *et al.* concluded that the maximum updrafts were correlated with the presence of the convergence at the base of the Tushar Mountains during the third stage. These updrafts were coincident with the areas of maximum water release. As the cold dome of the frontal surface rose with time, so did the updraft maxima, although the depth of cloud decreased due to a stable layer above the front, at 6 km MSL.

Sassen *et al.* (1990) utilized a combination of polarization lidar, C-band and Ku-band doppler radar, and scanning dual-channel radiometer data to describe the mesoscale structure and SLW characteristics of this same storm. The first segment of the storm as described above was distinguished by the development of an orographic liquid cap cloud at low levels as moist air was advected into the area from the southwest. This cap cloud was significantly affected by localized small-scale topographic effects, as maxima in SLW depth as seen by the radiometer were noted over small ridges surrounding the instrument. These localized maxima were incorporated into a larger-scale cap cloud which formed over the barrier as a whole. The maximum SLW content during this time was 0.22 gm^{-3} as measured by a surface SLW detector located at the higher reaches of the barrier. Precipitation was light, consisting of two short showers. In segment two, as the altostratus cloud became more potentially unstable, a series of generating cells were noted to move through the area. The largest reflectivity factors were found in association with these cells, and were seen to increase in the region near the barrier as they were orographically enhanced. Radiometer measurements of SLW indicated that these cells were effective in removing SLW from the lower orographic cloud. Zenith LW depths, found to be increasing prior to the period of cellular precipitation, were seen to decrease to near zero during episodes of strong echo and precipitation. Measured SLW amounts were $<0.05\ gm^{-3}$. As the surface cold front approached from the northwest in stage

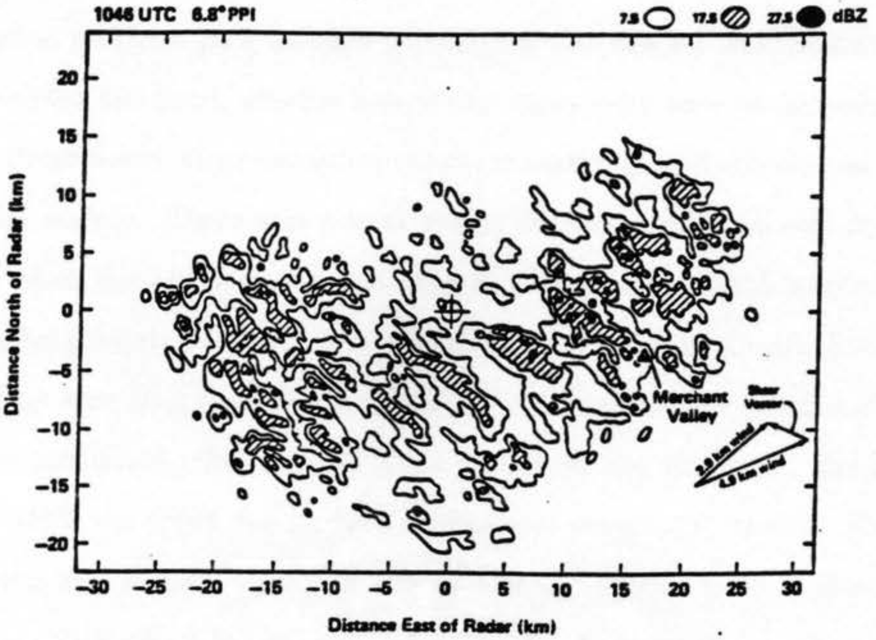

Figure 4: C-band radar 6.8° PPI display of DBZ for 1046 on 9 February showing convection within a mesoscale precipitation band. Wind vectors are from VVP (Volume- Velocity-Processing) analysis. The shear vector magnitude is ~ 6.5 ms^{-1}. The barrier runs parallel to the right-hand side of the figure, with barrier crest approximately 25 km east of the radar. (from Sassen *et al.* 1990)

two, an organized precipitation band moved across the area. This band was oriented northeast to southwest, and moved slowly to the southeast. A series of elongated convective cores moved within the band orthogonal to band movement (Figure 4). The cells within the band moved to the northeast at 18.0 m s^{-1} with a cell spacing of ~ 5 km, while snowfall at this time was heavily rimed and graupellike. A similar type of cloud band was associated with frontal passage. The frontal cloud was oriented southwest to northeast, and elongated convective cells within were oriented orthogonal to the band and moved to the northeast. These cells were spaced ~ 9 km apart and tilted eastward with height to ~ 3.5 km. Maximum reflectivities were in the layer between 4.0 and 5.0 km which was the convectively unstable layer. Precipitation trailed through the wind shear at lower levels. It was speculated that precipitation particles grew through accretion within the low level liquid orographic cloud. Behind the front, smaller reflectivity cores were seen to move in a similar fashion. Presumably, these cores formed as convectively unstable air was lifted over the frontal surface. There was a brief period between prefrontal and frontal band passage, when the radiometer noted that SLW values increased markedly, at one point reaching nearly 0.4 gm^{-3}, the high point of the storm. During band passage, SLW values were seen to decrease. After frontal passage, the banded structure of the storm continued. As the cold front moved to the southeast, the southwesterly flow aloft was lifted due to both frontal and orographic causes. The greatest reflectivities and highest echo tops were noted during this time. Volume-Velocity Processing (VVP)-detected updrafts were found to be coincident with or just ahead of reflecivity maxima, while SLW was seen to correspond to weak echo regions of the cloud, indicating that SLW would regenerate between bands. Precipitation during this time was heavily rimed. As the frontal surface ascended and ultimately rose above the barrier height, the region was cut off from moist southwesterly flow and precipitation subsided. The SLW cloud generated by orography was seen to be inefficient in terms of precipitation. The seeder-feeder process invoked by the transient bands was a major precipitation-inducing feature.

In another analysis of the same storm, Rogers *et al.* (1986) used vertically-pointing radiometer data to investigate some of the banded features noted in segment two of the storm. Spectral analysis of the one-minute resolution SLW radiometer series was performed (Figure 5). The most prominent peaks in the power spectrum are found at 12 and 6 minutes. Using the 4 km winds as steering level winds, a spacing of around 13 km between elements is found for the 12 minute peak. Superimposed on this feature were some smaller enhanced-reflectivity elements that were seen by the Ku-band radar. These elements had size and spacing of around

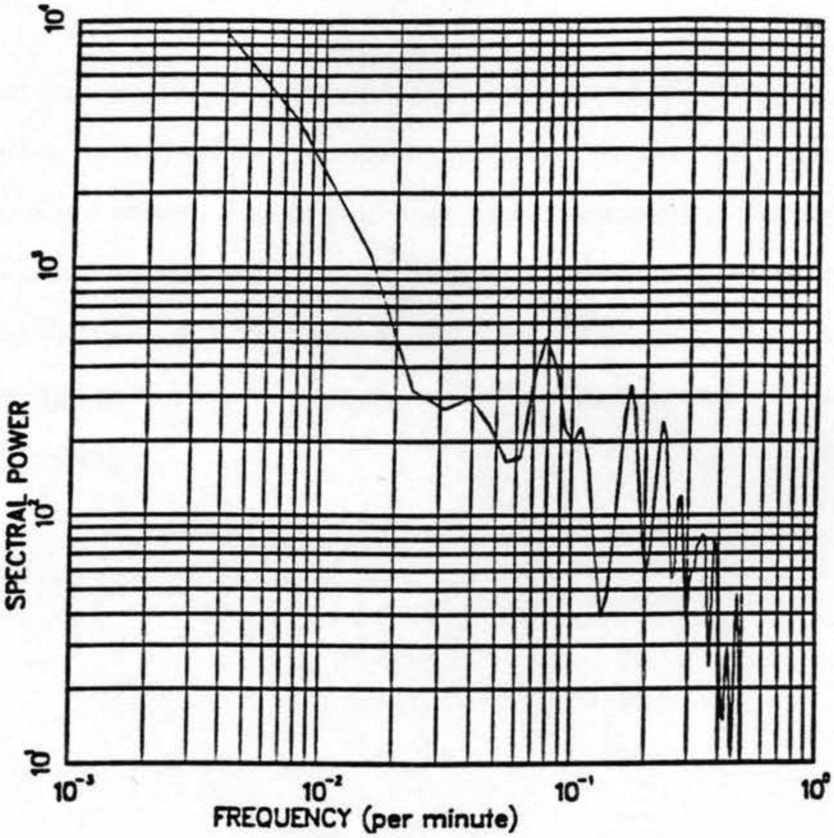

Figure 5: Spectral analysis of six hours of one minute resolution radiometer liquid water data. From Rogers *et al.* (1986)

2 km, which corresponds to the 6 minute peak in the power spectrum. The SLW maxima were found to exist about 1 km upwind of the reflectivity maxima. The description given was that as ice forms higher up in the cloud in a convective element, wind shear separates the reflectivity maxima from the SLW maxima lower in the cloud.

In the next few sections, data from a single case from COSE IV will be analysed and examined in terms of how it compares/contrasts to the body of orographic literature discussed above. The present case from northwestern Colorado will be seen to share some characteristics with orographic clouds in southwestern Colorado, Utah, and the Sierra Nevada. Differences will be noted as well, with the emphasis throughout being investigation of areas of enhanced reflectivity and/or cloud particle and SLW production.

3. RESEARCH SITE AND INSTRUMENTATION

The fourth COSE experiment was conducted from November 1984 through January 1985 in the Yampa River Valley in northwestern Colorado (Figure 6). The Park Range acts as a north-south barrier orthogonal to flow which is channelled up the east-west running valley, making the region ideal for the study of orographic clouds. COSE IV used a combination of aircraft, rawinsonde, remote sensor and surface data to study cloud characteristics and seeding potential. The general objectives of the COSE program (Rauber and Grant, 1985) were stated as follows:

1. Describe the microphysical processes governing the growth and development of precipitation in northern Colorado orographic clouds.
2. Quantitatively define the dispersion and transport of seeding materials in complex terrain.
3. Identify atmospheric covariates (predictors) which can be used in statistical analysis of weather modification programs.

During COSE IV, it was hoped that some of the questions raised in prior COSE programs could be addressed, as well as conducting research into airflow and precipitation processes over orographic terrain. One of the primary objectives for COSE IV was investigation of the distribution of supercooled liquid water (SLW) within orographic clouds and other microphysical characteristics involved with the growth and development of precipitation. Previous COSE studies had identified the three regions within orographic clouds in this study area where SLW was concentrated as cloud base, cloud top, and the region of maximum orographic lift near the barrier

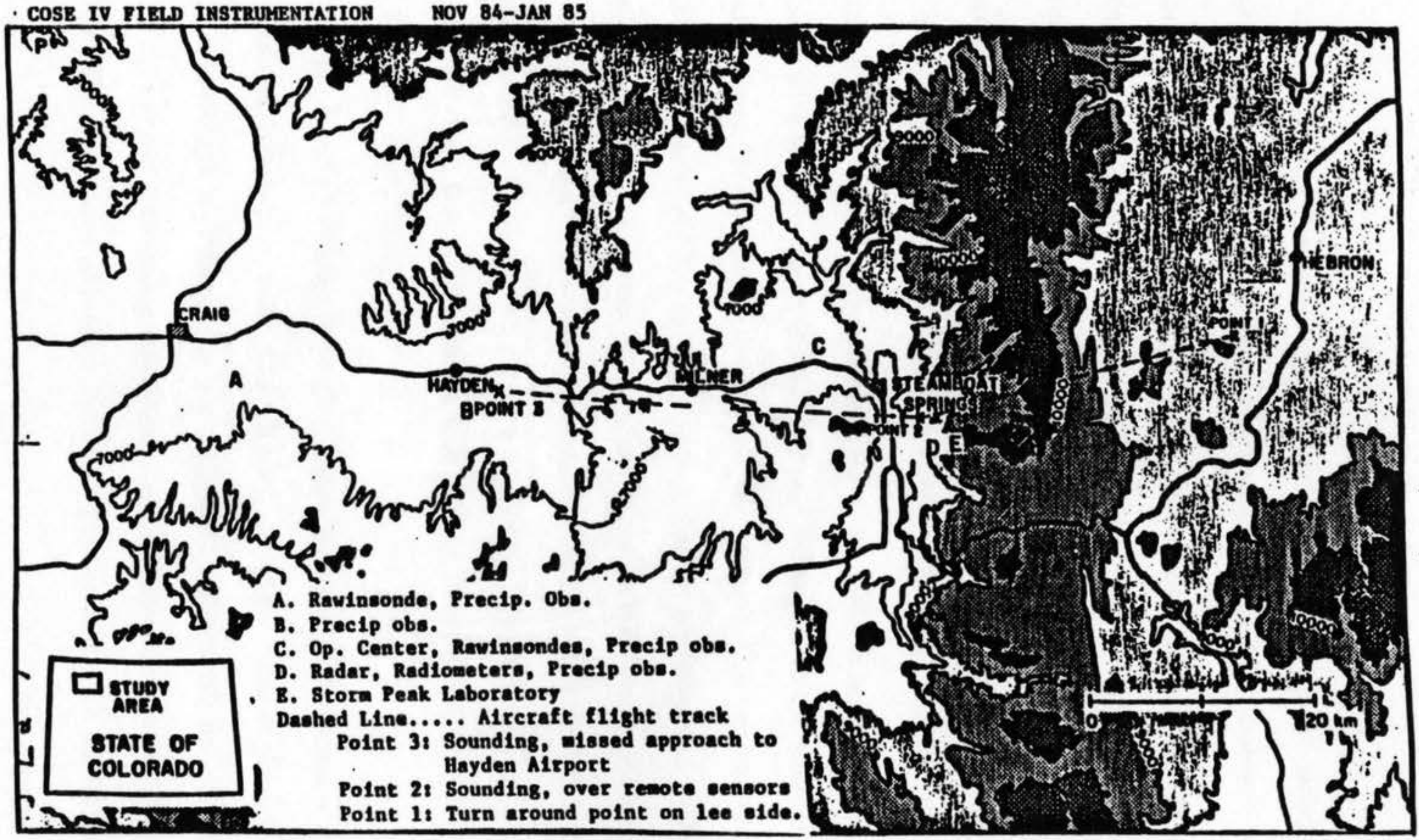

Figure 6: COSE IV study area near Steamboat Springs, Colorado.

(Rauber *et al.*, 1986). The instrument suite in COSE IV was situated in such a manner as to place these areas as much as possible under observation.

For the present case, rawinsonde, radar, radiometer, surface and aircraft data will be analysed to present a conceptual model of the precipitation and airflow characteristics for the orographic storm on November 28-29 1984.

Rawinsonde data were gathered at approximately 3-hour intervals during storm events at Craig (see Figure 6) by Colorado State University personnel.

A steerable dual-channel radiometer (Hogg *et al.* 1983, Rauber and Grant 1985) was colocated with a vertically-pointing Ku-band radar just to the south and west of Steamboat Springs (Figure 6), at the base of the barrier. The radiometer measures a path-integrated value of both liquid and vapor at frequencies 31.6 GHz and 20.6 GHz, respectively, and can be operated either in vertical or fixed-elevation azimuth scanning mode. Comparisons between radiometer and aircraft (Hill, 1992) and radiometer and sounding data (Martner *et al.*, 1993) have shown that quantitative values retrieved from the radiometer are generally in good agreement with data gathered *in situ*.

The CSU Ku-band (1.79 cm) radar (Rauber and Grant 1985, Greeson *et al.* 1979) was operated continuously in vertically pointing mode for most of the COSE IV period. This wavelength was chosen as the optimum wavelength for detection of ice particles in clouds not containing significant concentrations of large droplets (Greeson *et al.*, 1979). The radar averages together approximately 46 pulses per minute, to return reflectivity values for 200 range bins of 50 meter resolution. Rayleigh scattering is assumed, and reflectivity calculations are taken from Battan (1973). This assumption puts an upper limit on particle size of 1.7 mm (Sassen, 1987), which may be exceeded in regimes where graupel is prevalent or where aggregation is oc-

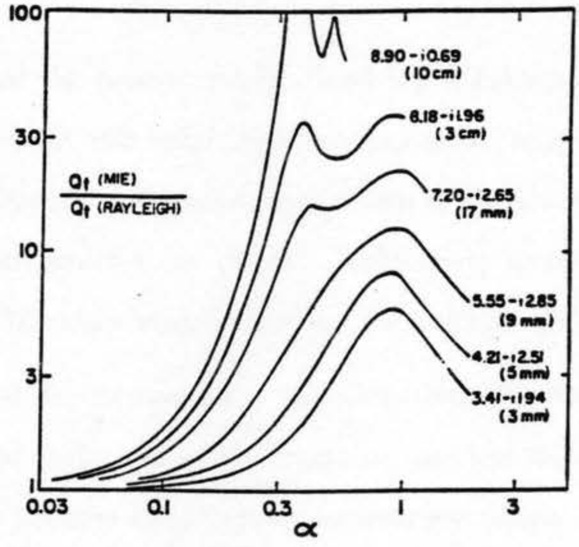

Figure 7: Ratio of Mie total scattering to Rayleigh total scattering by water spheres as a function of α. From Battan (1973).

curring. Figure 7, from Battan (1973), shows a comparison between Rayleigh and Mie scattering regimes, and it can be seen that if Rayleigh scattering is assumed in a Mie regime, then underestimation of the actual power backscattered will be the result.

The veracity of the radar data is further undermined by the fact that during COSE IV there was deterioration of the radar transmit-receive tube. A calibration was performed prior to the experiment, but another calibration was not performed until the following summer. A linear calibration curve was calculated, and the resultant factor was added to the reflectivity values during data reduction. However, the nature of the transmit-receive tube deterioration is not exactly known, so that the reflecivity values retrieved using the derived calibration factor are not exact.

Uttal *et al.* (1988) stated that the Ku-band radar was able to determine cloudtop to within 100-200 meters of that determined by observers in aircraft. Sassen (1987) shows that the Ku-band radar regularly underestimates cloud top height due to attenuation factors. For the present study, cloud top heights as determined from soundings were in agreement with heights retrieved by radar, which were in the range 5500 m msl. On the radar plots, contours were drawn at 10, 5, 0 and -5 dBZ values. Lower reflectivities were omitted for clarity. Reflectivity trends were accurately depicted, but actual dBZ values may be suspect, for the reasons mentioned earlier.

The National Center for Atmospheric Research (NCAR) Beechcraft King Air was available during the early part of the program, and the flight profile was such that the aircraft would perform soundings at prearranged points as well as fly transects through the cloud at various levels. Federal Aviation Administration (FAA) regulations required the aircraft to maintain flight levels above the Minimum Enroute Altitude (MEA), or 4200 m msl, which prevented the aircraft from sampling cloud base other than during missed approaches at Hayden (Figure 6), 40 km west of the barrier.

4. SYNOPTIC SITUATION

The classic orographic cloud situation for research and seeding according to the COSE IV *Operation Log* (Rauber and Grant, 1985) occurs during or just after trough passage associated with a Pacific frontal system. In this situation, there will be orographic forcing at low levels, with larger-scale subsidence aloft after trough passage. Figures 8-10 show the 70 kPa maps from 1200 UTC 28 November through 1200 UTC 29 November 1984. It can be seen that a trough moves through the area, with the trough axis over the research area between 1200 UTC on the 28th and 0000 UTC on the 29th. Figure 11 shows a time-height cross-section of the equivalent potential temperature (θ_e) profile and winds for the period 1200 UTC 28 November through 1800 UTC 29 November. This profile is a composite of data from soundings launched at Craig (Figure 6) and aircraft soundings performed over the Hayden airport. This profile indicates that an upper-level front passed through the research area at around 1500 UTC on the 28th. This is supported by surface snowfall measurements and radar data, which reveal highest snowfall rates and highest cloud tops at this time. The 70 kPa trough moved through the region in conjunction with the upper level front with an associated jet maximum, as seen in Figure 11. Within the scheme put forth by Rauber (1987) the orographic cloud and associated precipitation of the present case would be said to evolve from frontal to postfrontal. The θ_e profile indicates that some regions of the cloud were unstable (theta-e decreasing with height) during trough passage between 1200 UTC and 2000 UTC on the 28th, followed by a long period where the cloud was essentially neutrally stable.

Between 1500 UTC on the 28th and 0300 UTC on the 29th, measurements of low level winds from both Craig rawindsondes and aircraft soundings at Hayden

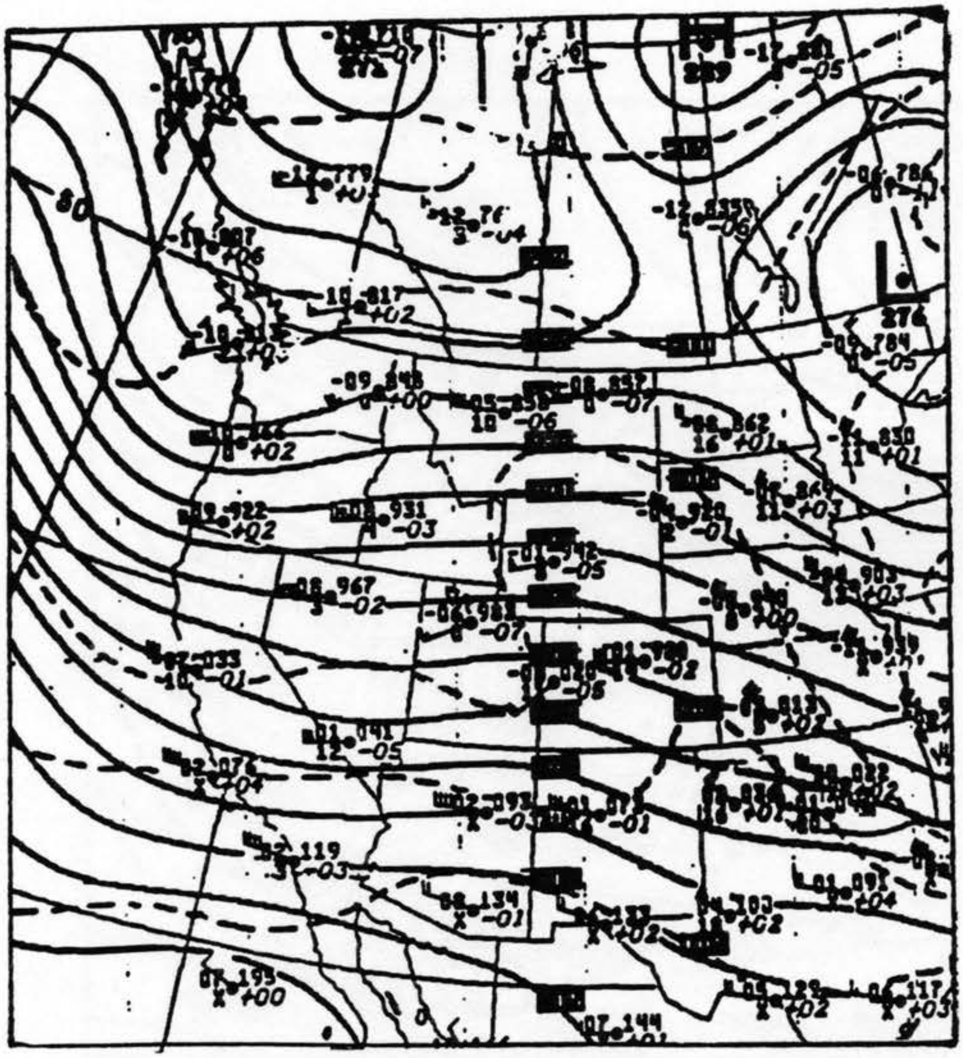

Figure 8: 70 kPa map. 1200 UTC 28Nov.

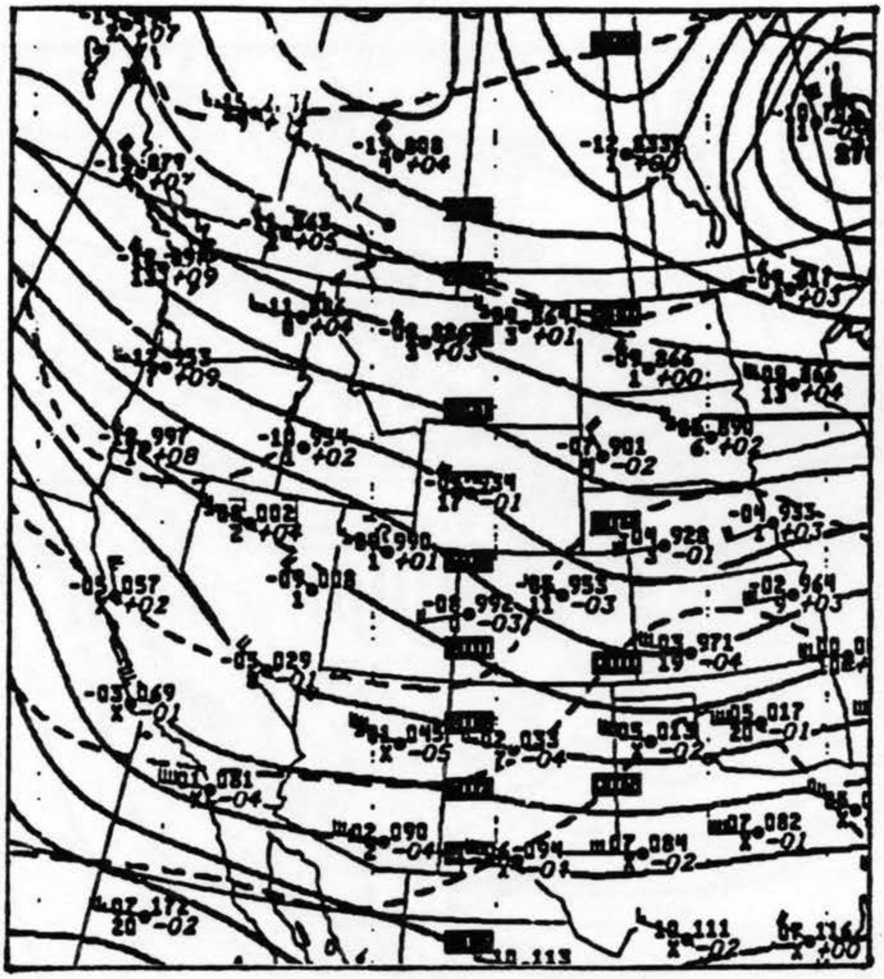

Figure 9: 70 kPa map. 0000 UTC 29Nov.

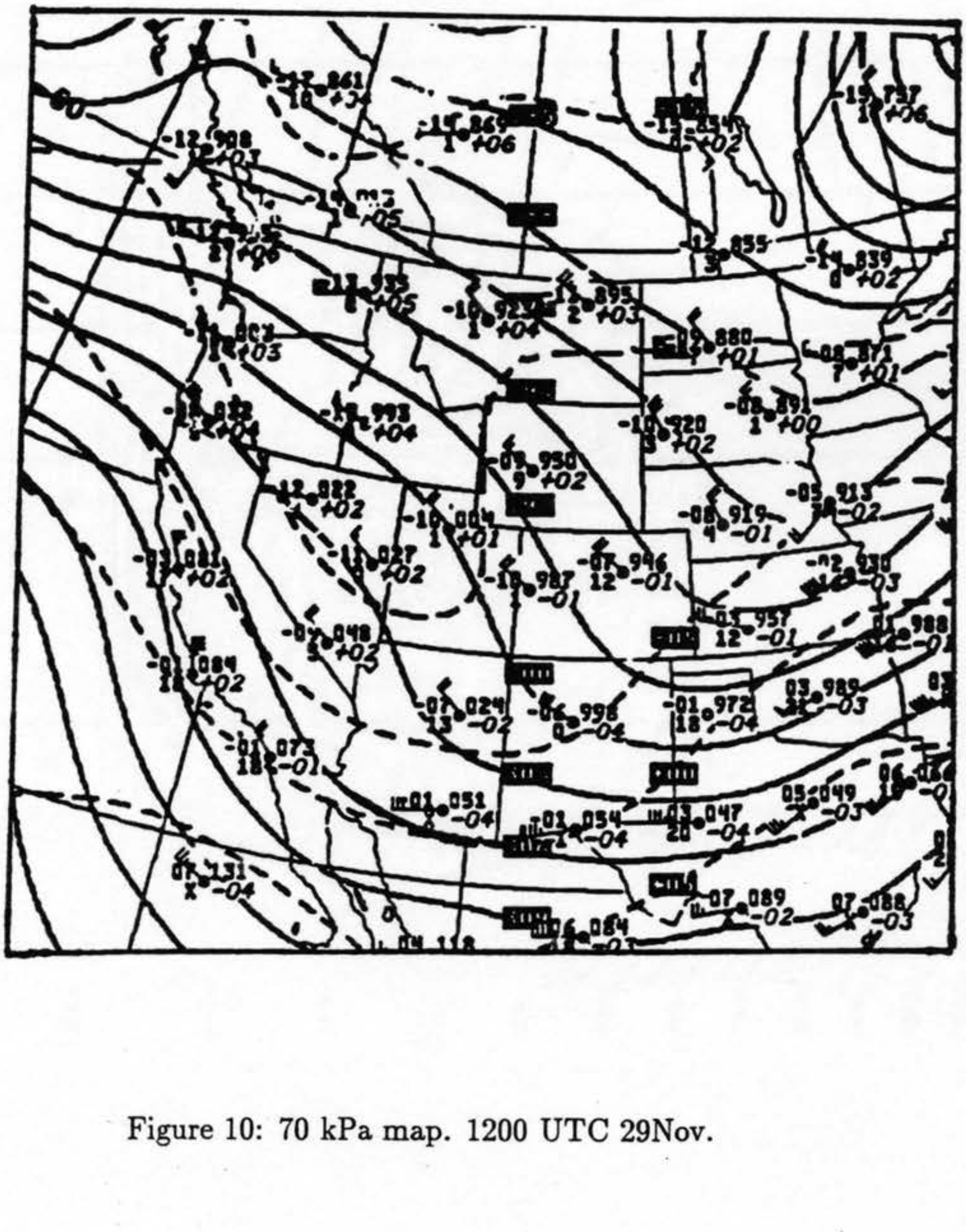

Figure 10: 70 kPa map. 1200 UTC 29Nov.

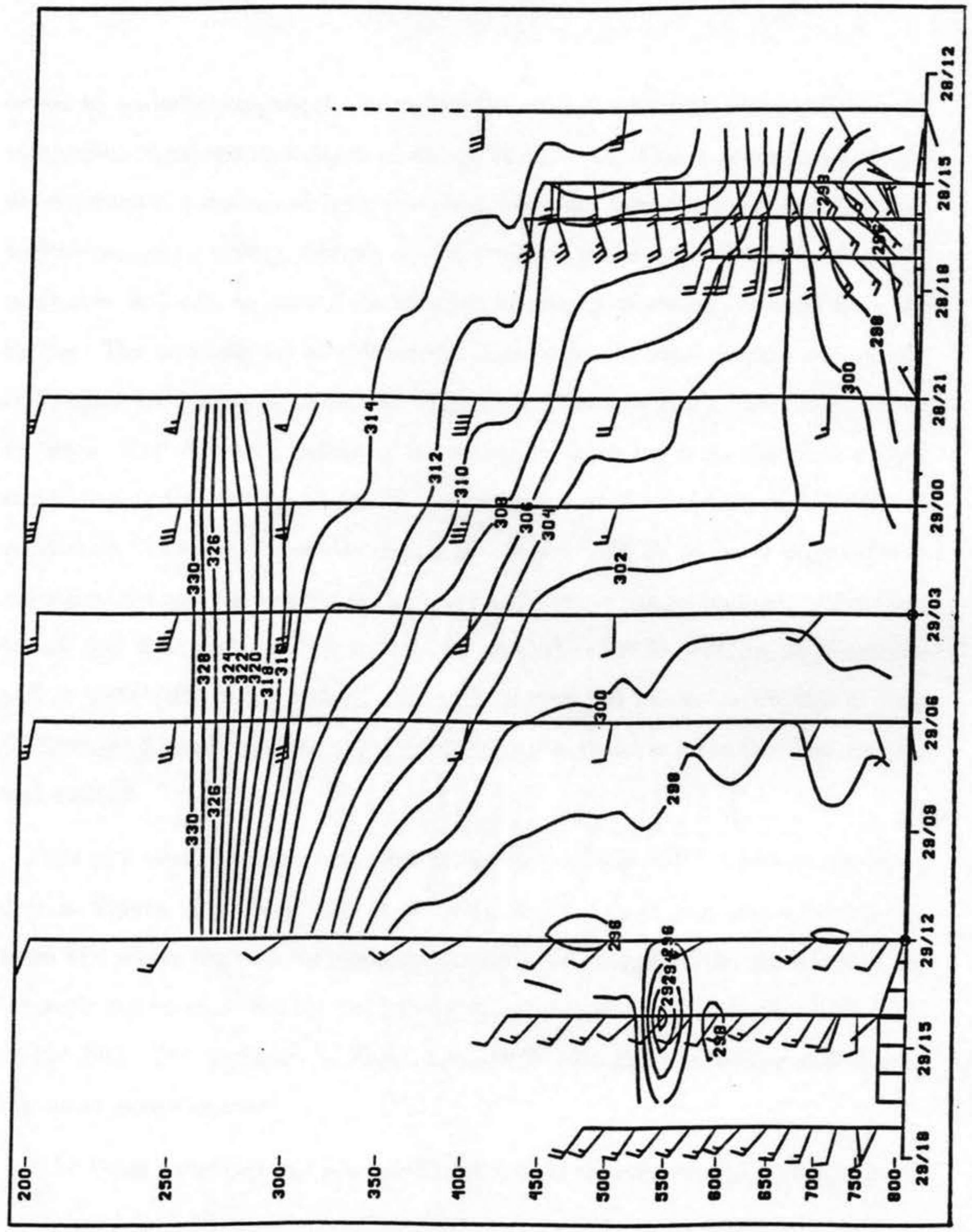

Figure 11: Time-height cross-section of θ_e and winds from 1200 UTC 28 Nov. to 1800 UTC 29Nov.

reveal an easterly component. Several of the aircraft soundings show this easterly component to extend to a depth of almost 500 meters. This is consistent with the development of a decoupled layer extending westward from the barrier as described by Peterson *et al.* (1991), wherein stable, low-level air becomes decoupled from the mean flow and acts to extend the effective orography westward, or away from the barrier. The development of a decoupled layer is not an uncommon occurrence in this region, happening in more than half of the total case study hours reported by Peterson. The westward extent of the decoupled layer has been shown to extend sometimes as far west as Craig (60 km upstream of the barrier), and further in some cases. The lack of a surface mesonetwork in COSE IV makes it impossible to determine the westward extent of the decoupled layer in the present case, other than to say that it extends at least as far west as Craig at 2100 UTC on 28 November and at 0300 UTC 29 November, with a depth near 500 meters at Hayden at 2100 UTC on the 28th. Regardless, the presence of a decoupled layer in this case appears well defined.

The plot of temperature and relative humidity (Figure 12) taken from the same data as Figure 11 gives an indication of the level of cloud top: the area from 47 to 50 kPa where the relative humidity gradient is strongest. Even though data are sparse, it can be seen that the thickness of the moist layer decreases after 0300 UTC on the 29th. The isotherms in Figure 10 indicate that there is cooling aloft during the entire period of study.

The Craig soundings can give additional insight into the evolution of this storm event. Figure 13, the Craig sounding from 1300 UTC 28 November, was taken when the atmosphere was pre-trough (see winds in Figure 11). Temperature is −10°C at 70 kPa, and almost isothermal to 55 kPa, where the temperature is −15°C. Temperature drops to −20°C by 50 kPa. The atmosphere is saturated from low

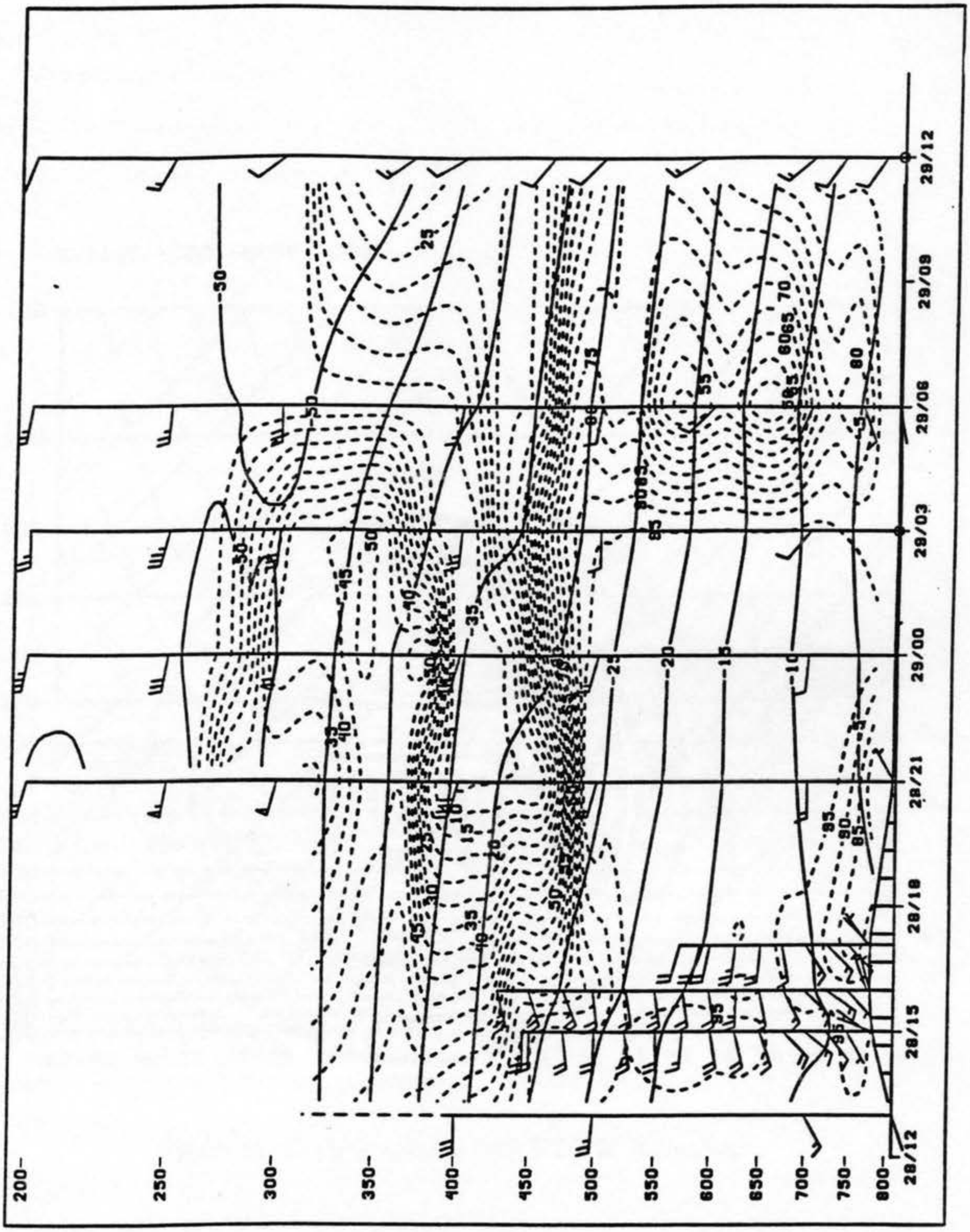

Figure 12: Time-height cross section of temperature and relative humidity from 1200 UTC 28 Nov. to 1800 UTC 29 Nov.

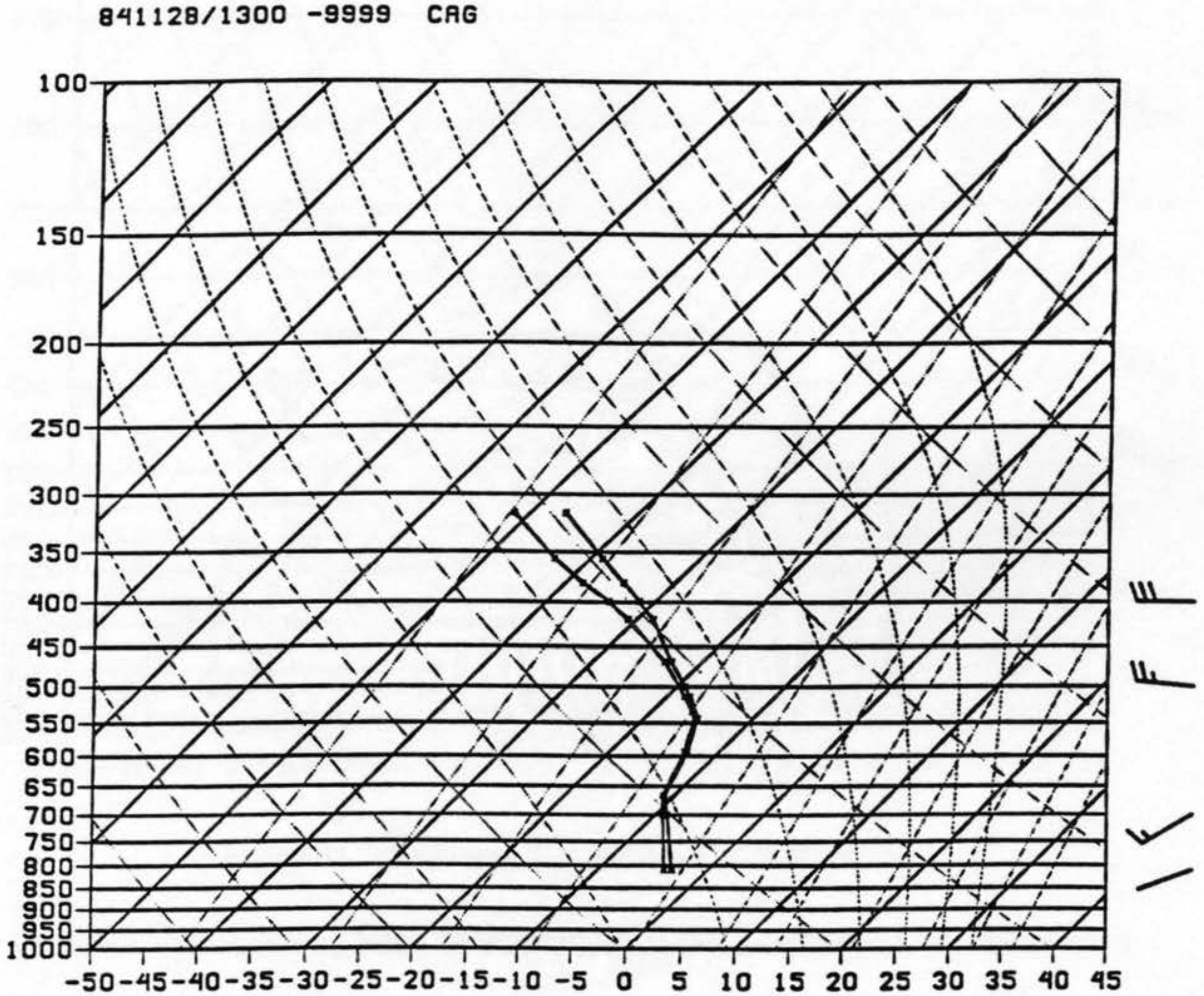

Figure 13: Craig sounding, 1300 UTC 28 November.

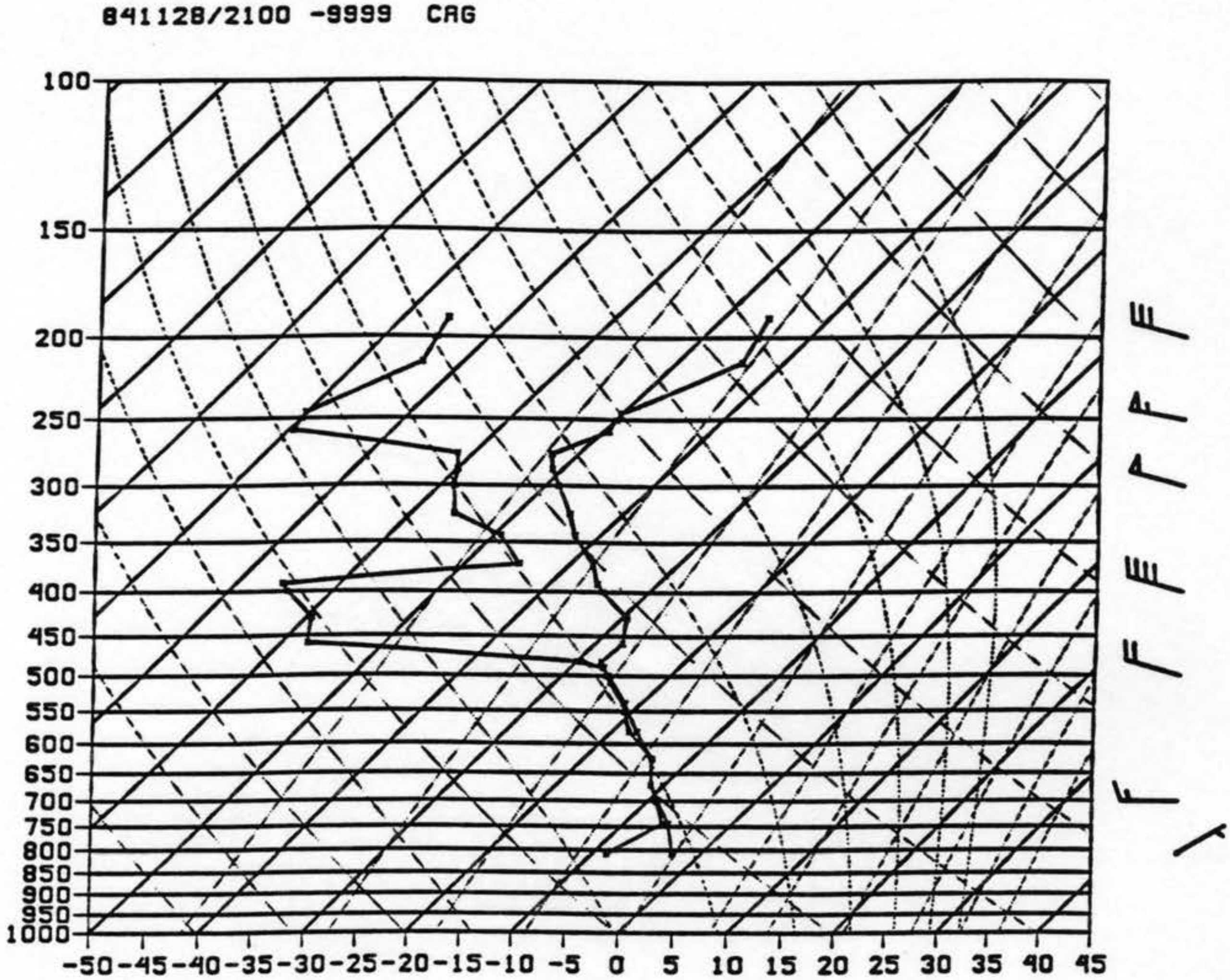

Figure 14: Craig sounding, 2100 UTC 28 November.

levels through almost 45 kPa. By 2100 UTC on the 28th (Figure 14), the effect of trough passage is readily seen. At 70 kPa the temperature is still near −10°C, but at 55 kPa it has dropped to −20°C, and to −25°C at 50 kPa. Above 50 kPa there is an increase in temperature evident of a subsidence inversion, while between 25-30 kPa strong winds indicate the presence of a jet. At the lowest wind level, the presence of the decoupled layer is supported by the fact that winds here are from the northeast, directly away from the barrier. Between 65 and 50 kPa, the atmosphere is nearly

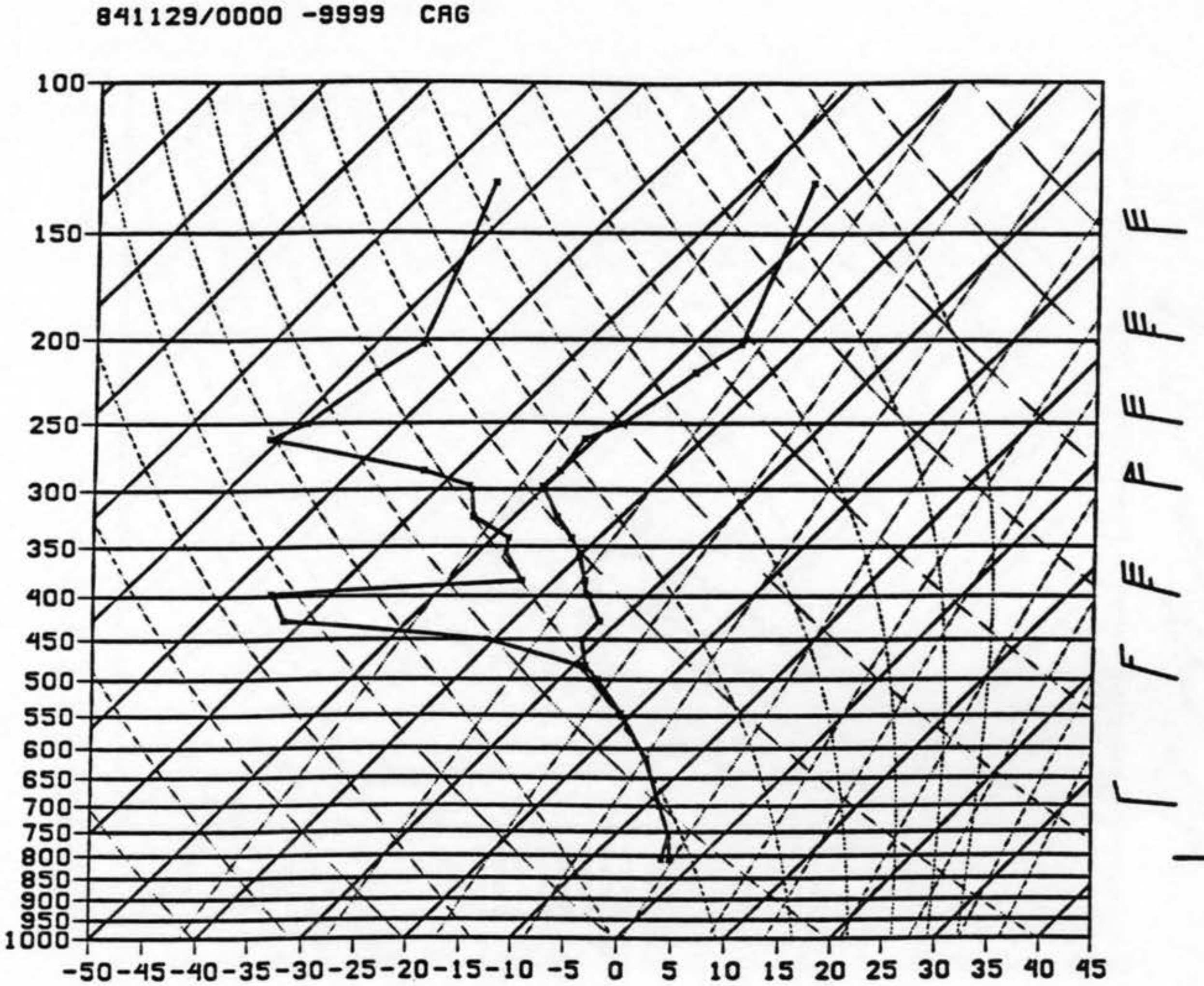

Figure 15: Craig sounding, 0000 UTC 29 November.

moist-adiabatic. At 0000 UTC on the 29th (Figure 15), the Craig sounding is quite similar to that taken at 2100. The atmosphere is nearly moist-adiabatic between 65-50 kPa, while the lowest winds are opposite those above, indicating that the lowest levels of the atmosphere are decoupled. Temperatures at 70 and 50 kPa are still −10° and −25°, respectively, while evidence of subsidence is seen aloft. At high levels, between 30 and 40 kPa there appears to be another moist layer at 2100 UTC on the 28th and 0000 UTC on the 29th. However, this layer is not ice-saturated, so

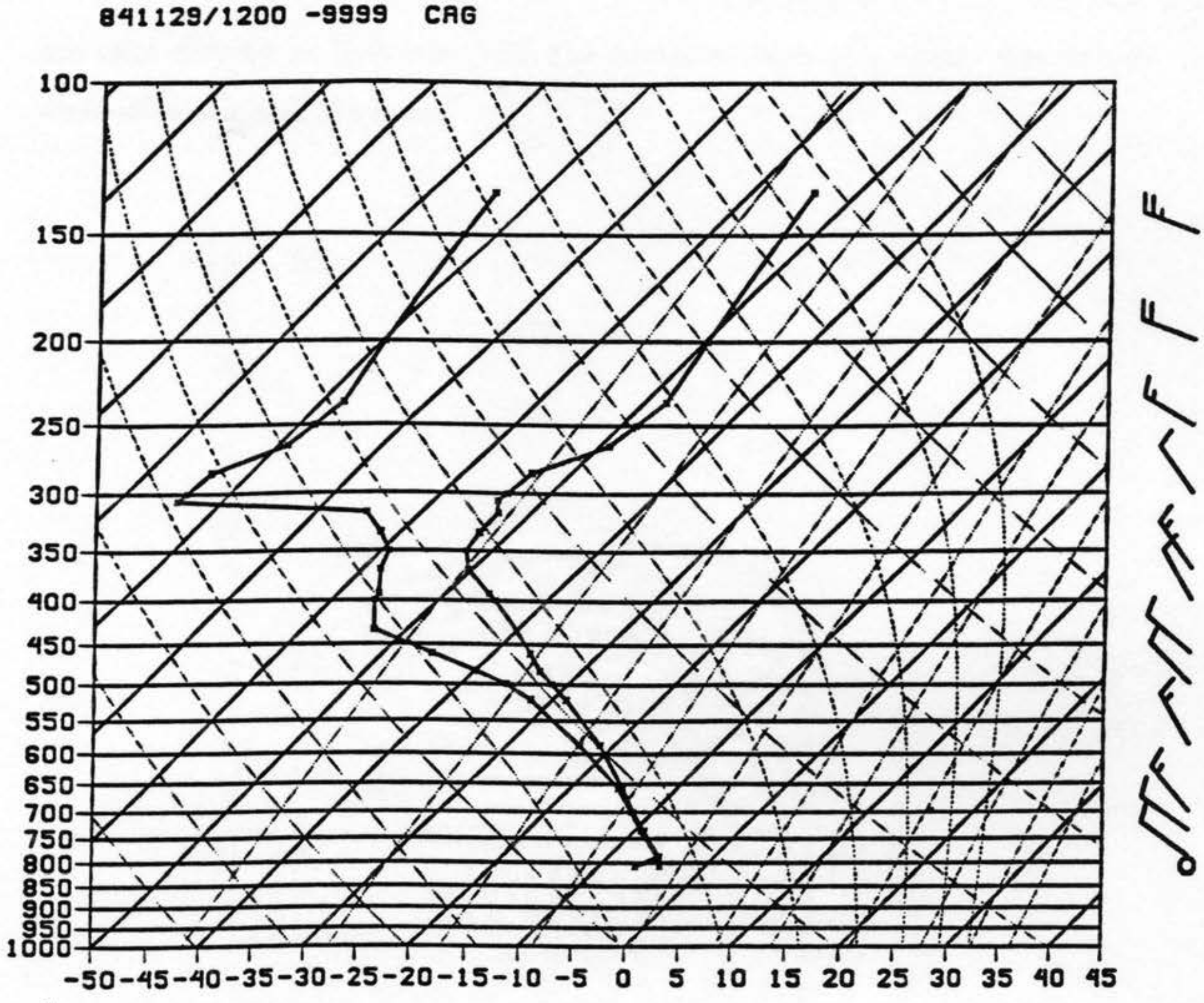

Figure 16: Craig sounding, 1200 UTC 29 November.

it is doubtful that there exists a seeder cloud over the orographic cloud of interest. Conditions remain essentially the same through 1200 UTC on the 29th (Figure 16), when it can be seen that the moist layer has become thinner, reaching only through 65 kPa. The atmosphere remains essentially moist-adiabatic through 50 kPa, but has cooled to −12° at 70 kPa, and −31° at 50 kPa. There is also no longer evidence of the subsidence inversion above cloud level at this time, while winds have weakened and veered to northerly, less of a cross-barrier component. That the lowest winds are calm may be an indication that the decoupled layer still exists, even in the dissipating stages of the storm.

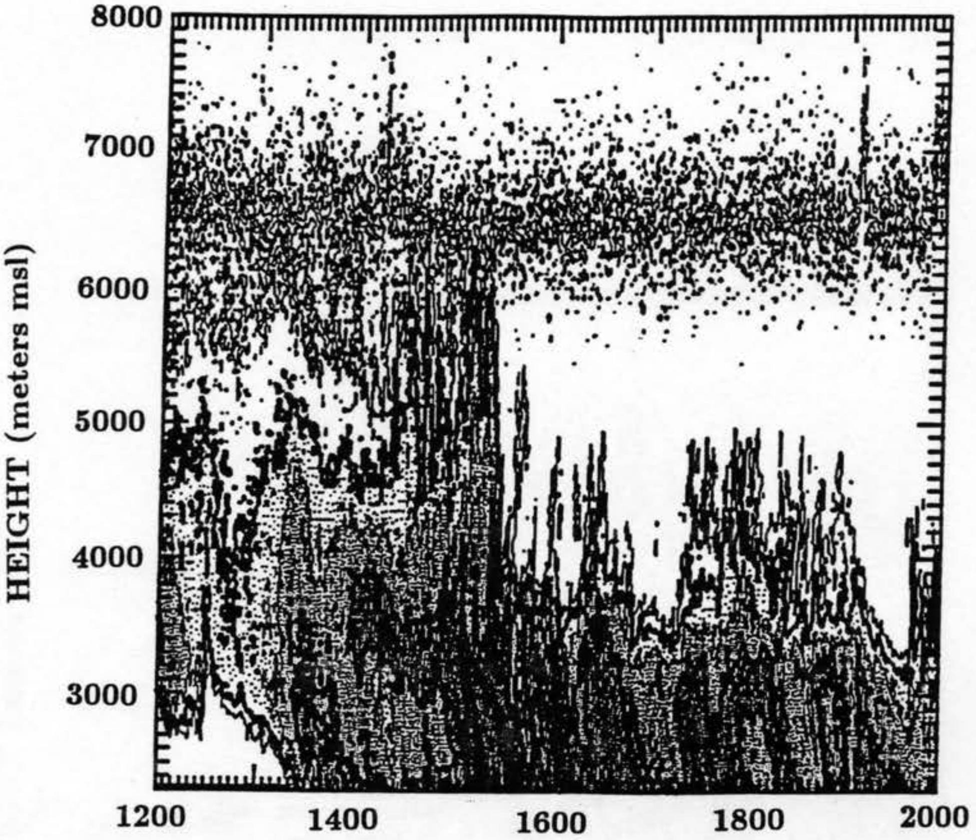

Figure 17: Radar reflectivity, 1200-2000 UTC 28 November. Bold lines represent 10 and 0 dBZ contours.

5. RADAR REFLECTIVITY DATA

The vertically-pointing Ku-Band radar was in continuous operation during the storm event. Figures 17-20 show 8-hour time-height segments of radar data. Postprocessing uncertainties incurred due to the deterioration of the transmit-receive tube as explained in Section 3 have made it difficult to ascribe precise reflectivity values to the radar output, so in the current study radar data will be used in a qualitative manner only. Trends recorded by the radar are accurate, however, so that the general trends represented are not in question. Darker shading in the figures represents areas of higher reflectivity.

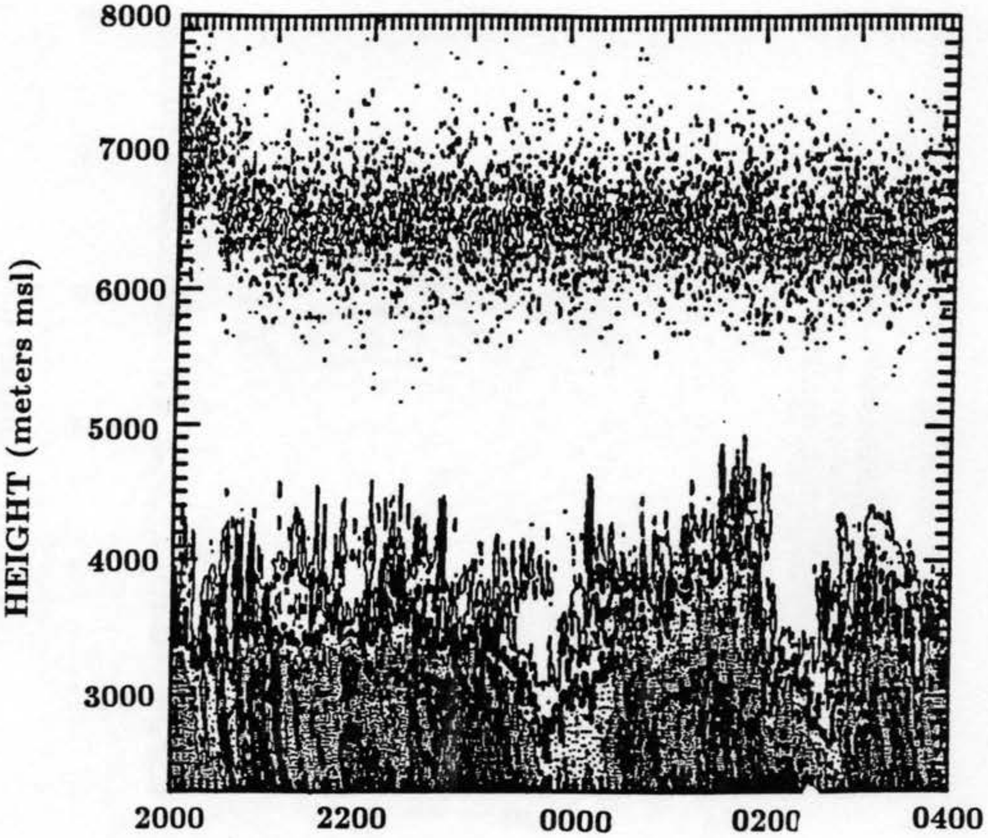

Figure 18: Radar reflectivity, 2000 UTC 28 November-0400 UTC 29November. Bold lines represent 10 and 0 dBZ contours.

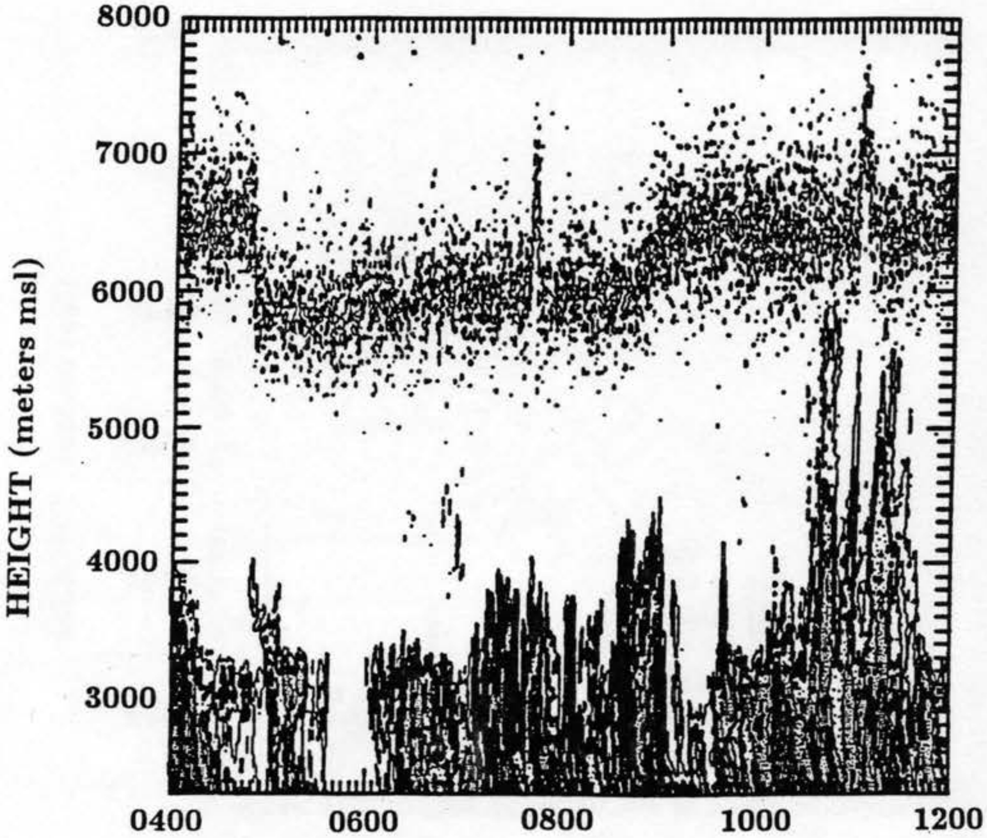

Figure 19: Radar reflectivity, 0400-1200 UTC 29 November. Bold lines represent 10 and 0 dBZ contours.

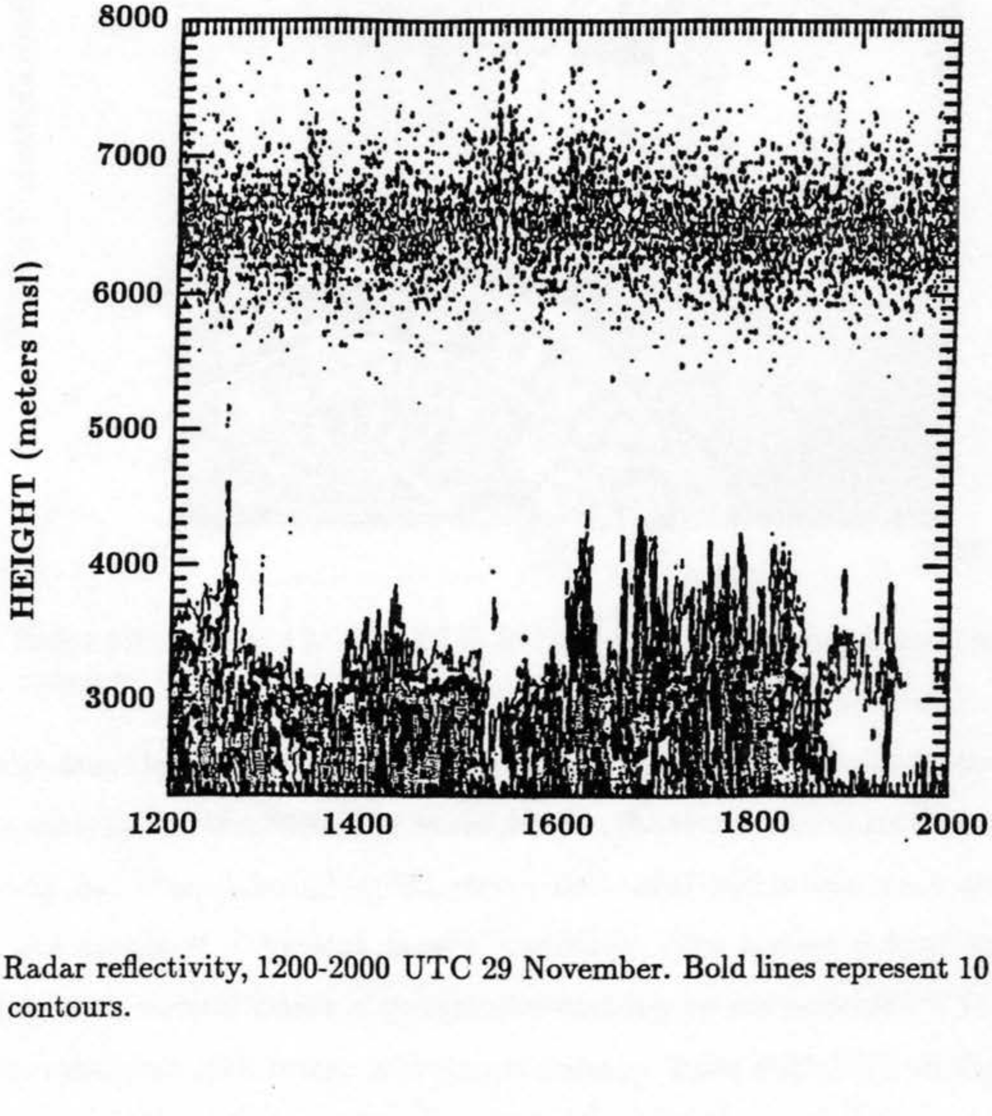

Figure 20: Radar reflectivity, 1200-2000 UTC 29 November. Bold lines represent 10 and 0 dBZ contours.

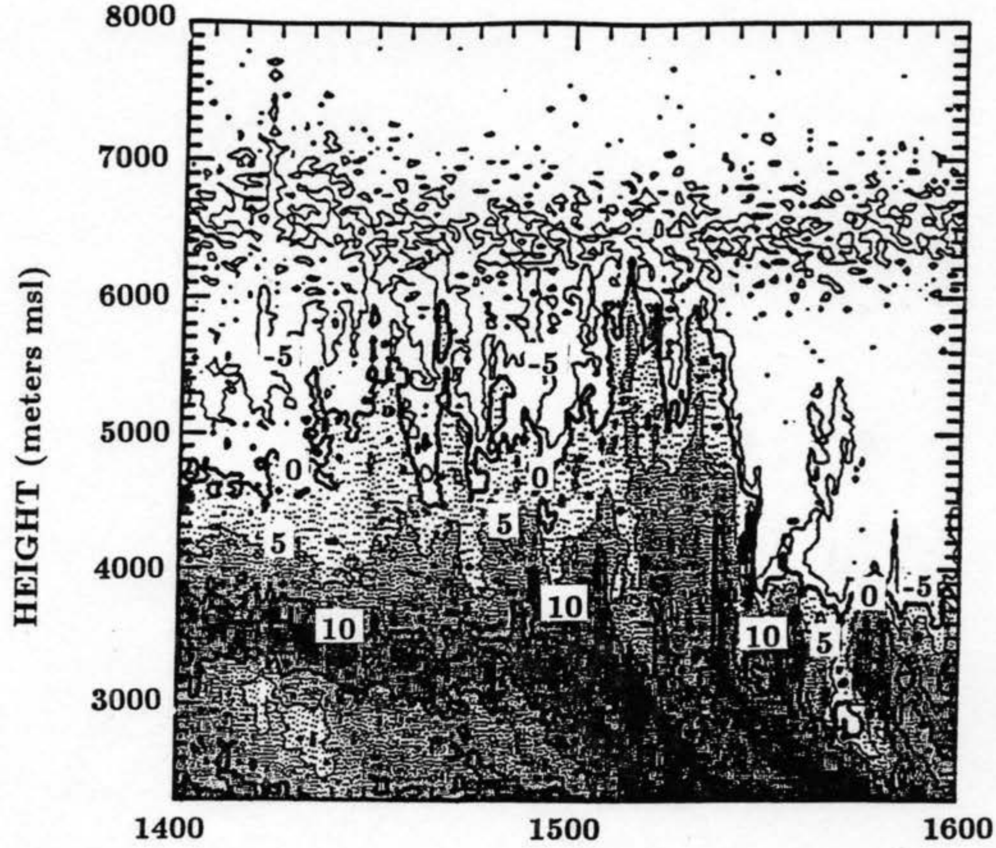

Figure 21: Radar reflectivity, 1400-1600 UTC 28 November. Bold lines represent 10 and 0 dBZ contours.

The radar data indicate a cloudtop of near 7000 m msl at the beginning of the storm, decreasing to between 6000-7000 m msl later in the event. This is consistent with sounding and aircraft levels for cloudtop. Embedded within the cloud are individual and groups of areas with higher reflectivity. The highest reflectivity values and greatest vertical extent of enhanced reflectivity occurs near 1500 UTC on the 28th, coincident with trough and frontal passage. After 1600 UTC on the 28th, there is an almost continuous progression of higher reflectivity elements past the radar. Figure 21 shows a more detailed view of the radar reflectivity for the period 28 November 1400-1600 UTC, corresponding to the time of trough passage. Between 1400 UTC and 1500 UTC there is a layer of enhanced reflectivity at a

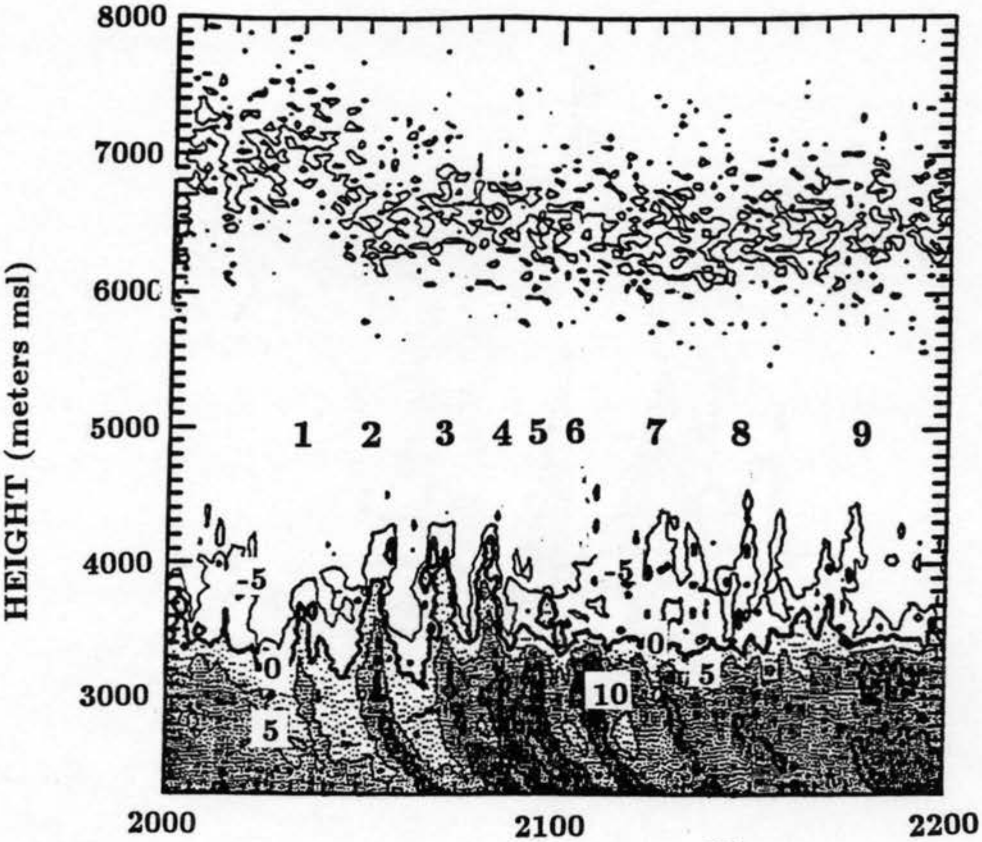

Figure 22: Radar reflectivity, 2000-2200 UTC 28 November. Bold lines represent 10 and 0 dBZ contours.

height of 3500 meters msl. Between 1450 UTC and 1545 UTC there is a sequence of three prominent enhanced reflectivity features that pass the radar. A consistent characteristic of the three features is the tendency for the enhanced reflectivity area to be vertically-oriented above 3500 meters msl, with the feature sloping downwards towards the ground below. The enhanced reflectivity aloft is the first to pass the radar, while the regions of the feature at lower elevations lags behind. Figure 22, a more detailed radar reflectivity plot for the period 2000-2200 UTC 28 November, shows that these enhanced reflectivity features persisted well past trough passage. Nine distinct features passed the radar during this two hour period, with fairly regular spacing, approximately 10-minute intervals, labelled 1-9 on Figure 22. The

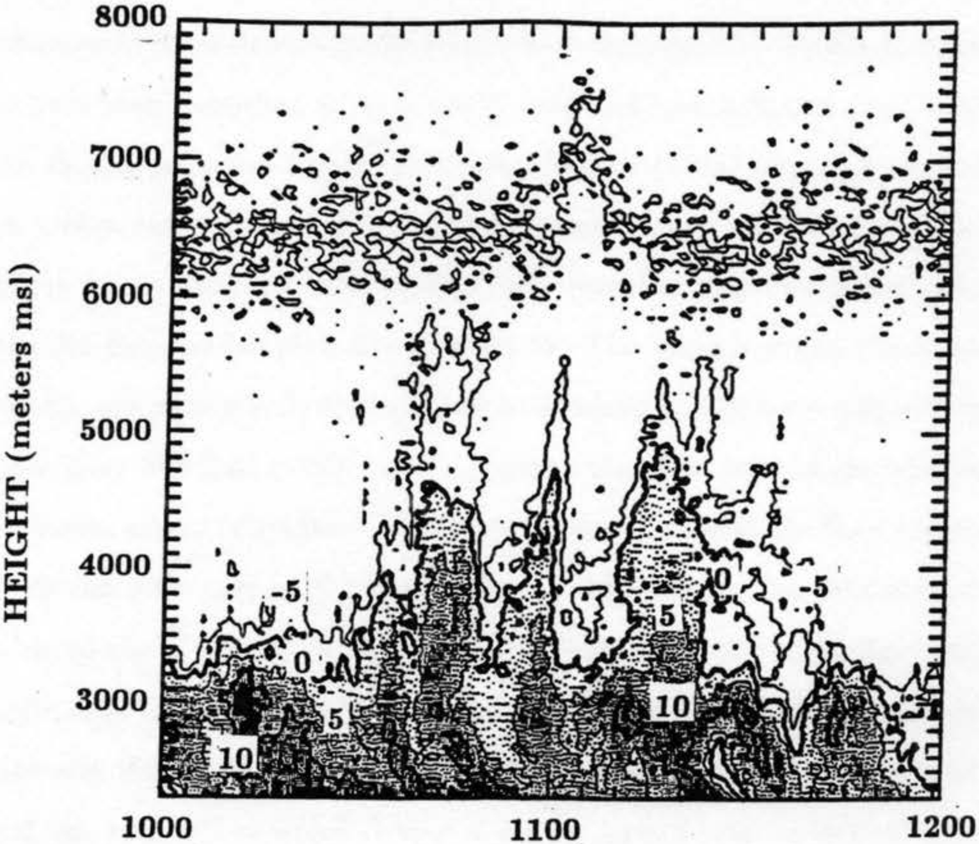

Figure 23: Radar reflectivity, 1000-1200 UTC, 29 November. Bold lines represent 10 and 0 dBZ contours.

morphology is similar to the features associated with trough passage, that is, a vertically oriented higher-reflectivity region aloft, sloping to the ground below 3300 meters msl. In Figure 23, a segment of the radar reflectivity from late in the storm (1000 UTC to 1200 UTC, 29 November) is shown. The same general morphology described above persists, with the enhanced-reflectivity features oriented vertically above 2800-2900 m msl and sloping to the ground below. After the element passed over the radar at low levels at 1020 UTC, it is easily seen that the features passed the radar at approximately 10-minute intervals. During the entire period of interest, these enhanced-reflectivity features were embedded within the orographic cloud.

Similar features to those described above have been described in a variety of cloud settings and have been described as 'generating cells' and 'precipitation streamers' for the lower, sloping region of higher reflectivity. Wexler (1955) describes banded precipitation embedded within widespread light precipitation associated with an extratropical cyclone. Wexler's RHI photographs reveal a structure remarkably similar to the Ku-Band radar plots from COSE IV. The sloping of the streamers pendant from the generating cells was ascribed to windshear. The term 'generating level' was coined by Marshall (1953), who suggested that this level is the level at which precipitation either originates or grows to detectable levels. Ludlam (1956) investigated similar streamers or 'fallstreaks' from cirrus clouds. The formation of cumuliform 'shred-cloud' over the region of the fallstreaks suggested to Ludlam that latent heat release could induce vertical motion in the region of the fallstreaks. Data from the winter of 1954 at Montreal reported by Douglas *et al.* (1957) reveal that a majority of the snowfall recorded during a 7-week period was associated with generating cells and fallstreaks. Often, these cells occurred just above a frontal surface, in hydrostatically stable air. Douglas *et al.* also suggested latent heat release as a mechanism to induce vertical motion. Wexler and Atlas (1959) describe a cellular pattern associated with dry air aloft ahead of a trough. The convective instability would transform a region of uniform echo into a cellular pattern, where initially cells would form, evolving into cells with fallstreaks, and eventually into fallstreaks without generating cells. These cells were found to move at the speed of the winds at their lowest level-the generating level. Hobbs and Funk (1984) observed generating cells and fallstreaks with a Ka-Band (0.86 cm) radar, from a variety of synoptic situations, both pre- and postfrontal as well as in a seeded altocumulus deck. Again, the slope of the streamers was ascribed to shear.

Within the context of the conceptual model of the generating cell put forth by the preceding authors, it is possible to extrapolate some information from the COSE IV Ku-Band radar data presented in Figures 21-23. First, it is not possible at this time to describe the enhanced reflectivity features seen on 28-29 November 1984 as either 'bands' or 'cells'. The vertically pointing radar was the only radar in the area, and available satellite views do not have the resolution to permit inspection of features on this scale. A 5-cm radar located 25 km west of the barrier during COSE III, in 1981-82, indicated that banded features oriented parallel to the barrier moved through the network at times. However, radar coverage and scan strategies did not permit a comprehensive climatology on the nature and prevalence of these banded features, as elevation angles were commonly too high to provide areal coverage of very much of the orographic cloud, and at low elevation angles ground clutter dominated the signal returned. In several cases, however, a band could be tracked moving from west to east through the area of cloud sampled by the radar, indicating that bands moving through the cloud are a definite occurrence.

As the effect of windshear has been reported as being responsible for the sloping aspect of the fallstreaks, it seems likely that the top of the sloping fallstreaks from the COSE IV dataset represent the vertical extent of the decoupled layer. This depth was seen to be at about 500 m above the ground in the Hayden-Craig area, and so can be expected to be at a higher level at distances closer to the barrier. Above this decoupled layer the whole reflectivity pattern moved with the winds, and was vertically oriented as shear within this layer was negligible. As precipitation particles fell into the calm or light winds in the blocked flow, they were in effect 'left behind' the generating cell as it neared the barrier. If the orographic cloud is assumed to be steady-state, this can be seen by picturing the radar plots of Figures 17-23 as being an east-west cross-section viewed from the north. Looking vertically from the radar, an observer sees the enhanced reflectivity associated with the generating band or cell 10 to 15 minutes before the effects of that same reflectivity area are manifest as increased snowfall rate at the ground. Surface snowfall measurements support this, as the highest snowfall rate during the period was associated with the large bands or cells that passed through the network in conjunction with trough passage around 1500 UTC on the 28th. Subsequent snowfall measurements are positively correlated with the presence or absence of the enhanced-reflectivity features, although the time resolution of the measurement was not small enough to catch individual events except in one or two instances where spacing between bands was large in space and time.

Wexler and Atlas (1959) contend that generating cells move with the winds at the generating level. By taking the top of the decoupled layer at 3000-3500 meters msl as the level where the enhanced-reflectivity elements' orientation changes from vertical to sloped as the generating level, we can retrieve an estimated speed for these cells by assuming they move with the winds at this level. Elevations of 3500 meters msl and 3000 meters msl correspond to pressures 650 and 700 kPa, respectively. Winds in this layer varied during the storm event from 10 to 20 m s^{-1} according to aircraft observations. Taking 15 m s^{-1} as an average value, we can estimate that if individual enhanced-reflectivity elements were passing the radar at a rate of one every 10 minutes that they were 9 or 10 km apart, while elements passing the radar every 20 minutes would be 18 to 20 km apart. Similarly, a feature that takes 5 minutes to pass the radar will be approximately 5 km wide. For the present case, individual elements have intervals as long as 45 minutes (40.5 km) and as short as several minutes (less than 1 km). Cell or band widths vary from near 5 minutes (4 km) to 35 minutes (31.5 km). A common occurrence is for a long period of inactivity (30-45 minutes) to be interrupted by a period where numerous enhanced-reflectivity elements pass the radar with short interval times, often less than 10 minutes. This can be seen in Figures 18, 19 and 20.

In the following section aircraft data will be analyzed to determine if these areas of enhanced reflectivity can be characterized by larger ice particle sizes, greater numbers of particles, or both. Radiometer data will be investigated in a later section as well.

6. AIRCRAFT OBSERVATIONS

The NCAR King Air made two flights through the COSE area during the storm period. The first was between 1450-1750 UTC on 28 November as part of a natural cloud system study, and the second was between 1340-1715 UTC 29 November as part of a seeding operation. Upon landing, however, it was found that the ignition wire was broken and the seeder tanks were empty. Therefore, it was not known whether or not the seeding material was effectively ignited. The microphysical data do not exhibit the characteristic 'seeded' features of very large number concentrations, so it is assumed for this study that the cloud was not seeded. Therefore the data from this second flight can be classified as a natural cloud study as well, and effects due to cloud seeding can be discounted. The King Air carried a full suite of instrumentation, including instruments for measuring particle habit and size spectra. These were the Particle Measuring Systems' model FSSP-100 (operated in 2-32 μm range with 2μm resolution) PMS model 2D-C (50-1600 μm range 50μm resolution), and a PMS model 2D-P (200-6400 μm range, 200 μm resolution). Crystal concentrations, sizing and other information are calculated on the basis of shadow pattern and buffer storage capacity. Rauber (1987) describes some examples of artifacts in imaging that can result in spurious data values. For the present study, images from the 2D-C and 2D-P probes were inspected visually for artifacts to reduce the chance for questionable data to be included. FSSP data were averaged into 1-minute bins from which spectra were calculated; shorter averaging times were not available. In this analysis aircraft data from horizontal flight legs perpendicular to the barrier were used in an attempt to determine if spatial differences in cloud microphysical characteristics could be found and correlated with the radar data. Additionally, data from different flight levels were compared with each other.

6.1 SUPERCOOLED LIQUID WATER

The airspeed of the King Air was generally around 100 m s^{-1}, so that each 1-minute FSSP spectra represented approximately 6 km of data. Therefore, it is possible that if a 5 km wide feature is to be sampled, the averaged FSSP spectra could mask some of the drop size spectral characteristics if the centerpoint of the averaging period represented the transition point from an area of increased cloud activity to an area of lower activity. For that reason, spectra from transitional zones in the cloud were avoided in the analysis. There was a recurring variation in the FSSP spectra that could be seen at all flight levels. Figure 24 Shows some representative FSSP spectra from the four heights at which horizontal flight legs were flown. All data in Figure 24 were at a distance of greater than 30 km west of the barrier. Figure 25 is identical to Figure 24 except that all spectra here were taken from cloud less than 30 km west of the barrier. The left hand columns of Figures 24 and 25 are representative of what are termed 'active' regions, that is, areas where there is liquid water being produced. This is indicated by a peak in the spectra in the 6-12 μm range, revealing that new drops are being nucleated. The right hand columns in Figures 24 and 25 represent 'inactive' regimes, or regions where the concentrations in the 6-12 μm range are one to four orders of magnitude lower than in the active regions. SLW spectra in these regions are either shifted to the right as droplets grow larger, or are depleted at all sizes as SLW is accreted or evaporated without production of new droplets.

While flying a horizontal path normal to the barrier, the aircraft would sample both active and inactive regions of the cloud. This suggests two different types of regimes within the cloud, one where vertical motion was significant enough to produce SLW, and one where liquid was either not being produced or was being

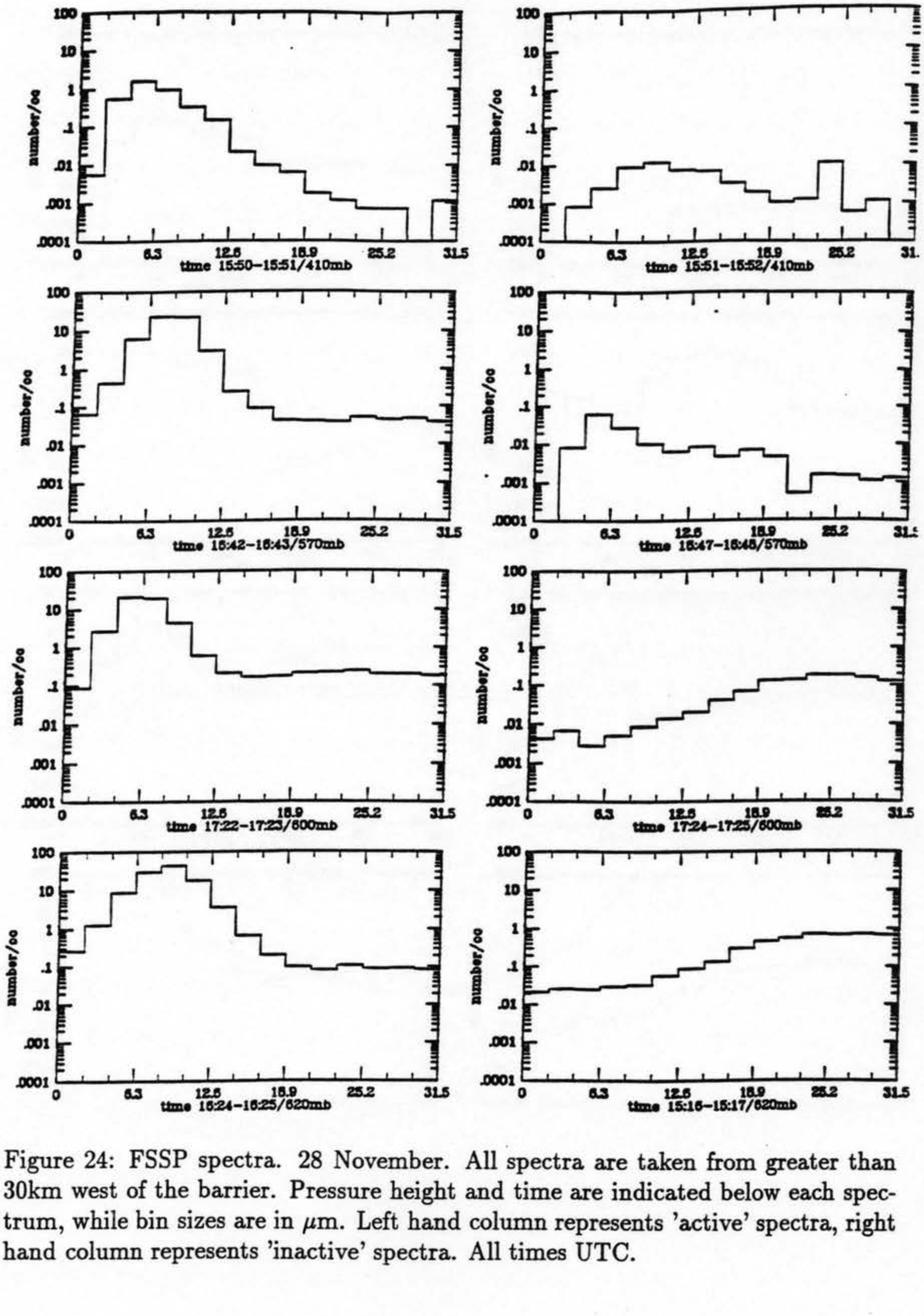

Figure 24: FSSP spectra. 28 November. All spectra are taken from greater than 30km west of the barrier. Pressure height and time are indicated below each spectrum, while bin sizes are in μm. Left hand column represents 'active' spectra, right hand column represents 'inactive' spectra. All times UTC.

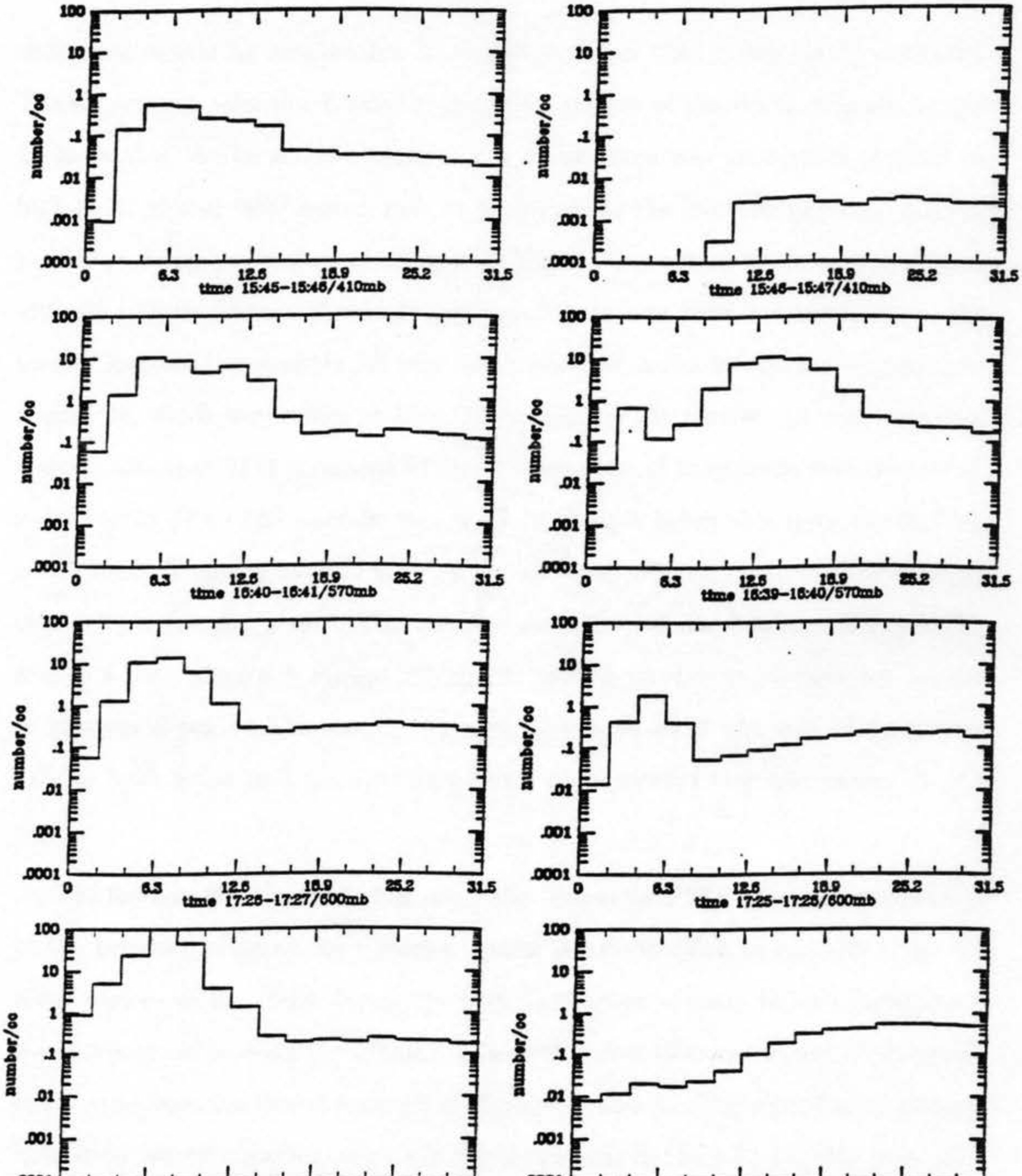

Figure 25: Similar to Figure 24, except all spectra are taken from from less than 30 km west of the barrier.

consumed, either by evaporation or accretion, faster than it was being produced. These processes were not limited to the lower regions of the cloud. Figures 24 and 25 show that in the active regions of the cloud there was production of SLW as high as 41 kPa or 9000 meters msl, as evidenced by the concentrations in the 6-12 μm range being two orders of magnitude higher than others taken from the same altitude (Figure 24-top, Figure 25-top). Active regions were not restricted to the area of increased orographic lift near the barrier, as shown by the active spectra in Figure 24, which were taken at least 30 km west of the barrier. In active regions, concentrations of SLW increased by one to two orders of magnitude with decreasing height to 62 kPa. The aircraft was unable to sample below this level due to FAA restrictions. There appears to be a tendency for the spectral mode to shift to larger sizes with decreasing height. This can be seen in the left hand column of Figure 24, and to a lesser degree in Figure 25. The distance from the barrier does not appear to have an impact on the spectra. Spectra from as far as 50 km west of the barrier exhibit both active and inactive signatures, while spectra near the barrier do the same.

The flat size distribution in the larger size bins of the FSSP spectra are indicative of the presence of small ice particles within the cloud (Vali *et al.*, 1981). In the lower regions of the cloud during the first flight there appears to be a background concentration of between 0.1-1.0 cm^{-3} at heights below 4500 meters msl. This can be easily seen from the lowest 4 panels of Figures 24 and 25. The right-hand columns, indicating inactive regions, show low concentrations in the 5-12 μm size bins, with concentrations an order of magnitude higher at sizes greater than 15 μm. Figures 26 and 27 show FSSP data from the flight on 29 November 1430-1715 UTC. These data are similar to those from the earlier flight, with some minor differences. The shift in mode in the active spectra towards larger sizes with decreasing height is not

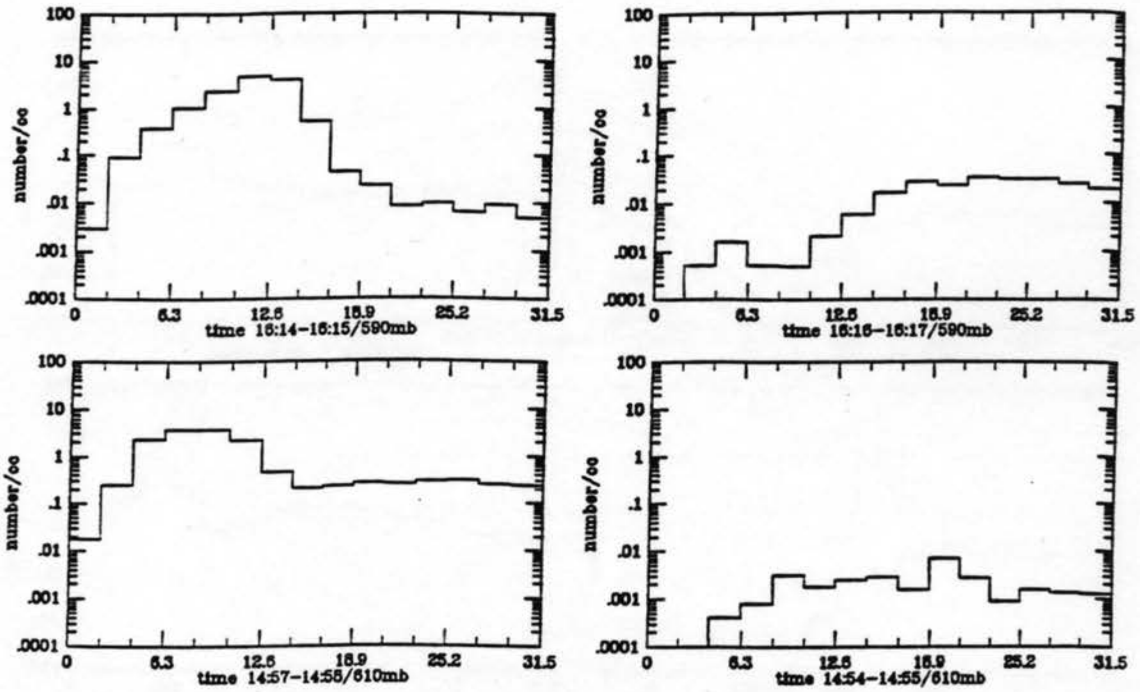

Figure 26: FSSP data. 29 November. All spectra are taken from greater than 30km west of the barrier. Pressure height and time are indicated below each spectrum, while bin sizes are in μm. Left hand column represents 'active' spectra, right hand column represents 'inactive' spectra. All times UTC.

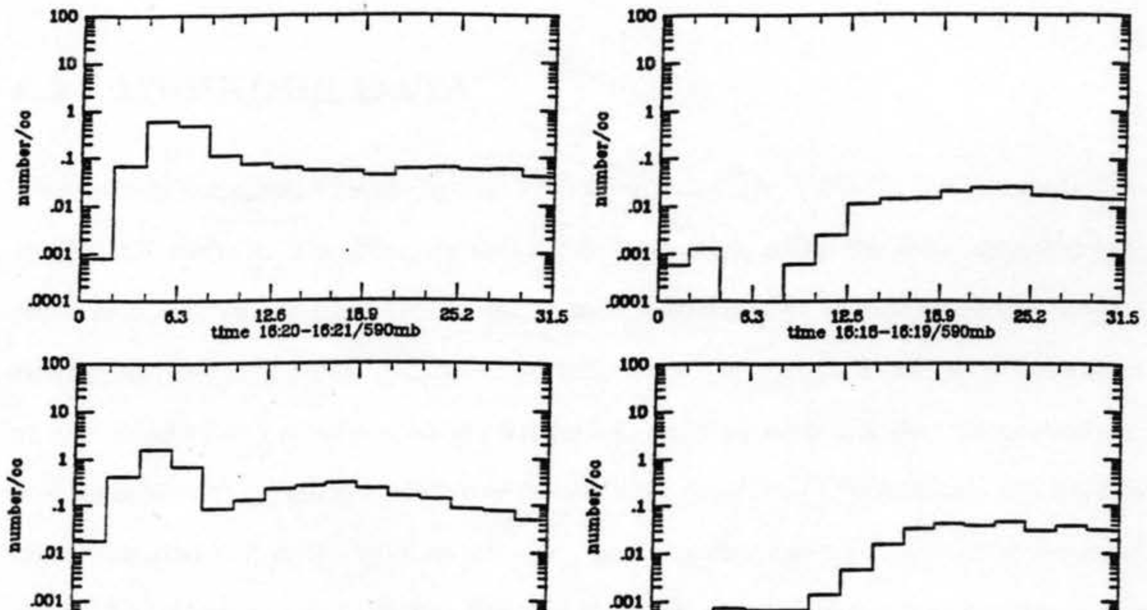

Figure 27: Similar to Figure 26, except all spectra are taken from less than 30 km west of the barrier.

found. This may be due to the fact that the two horizontal flight tracks from 29 November were only 200 m apart in height, so that essentially the same region of cloud was being sampled in each case. The concentration in the larger size bins, or background ice concentration was not consistent in the later flight. This can be noted in the FSSP spectra in the lower right hand corner of Figure 26, and may be due to the fact that during the second flight the cloud was in its dissipating stages, while the first flight came during the most vigorous stage of the storm.

6.2 2D-PROBE DATA

Two two-dimensional Cloud Optical Array Probes (2D-C, 2D-P) were mounted on the NCAR aircraft. The 2D-C sampled cloud particles, while the 2D-P sampled particles of precipitation size. Due to incompatibility between stored aircraft data and processing software, investigation of particle data was restricted to use of microfilm of raw images and pre-calculated parameters such as total number concentration, and numbers and concentrations of plates and dendrites (determined by shadow characteristics). Averaging of spectra was not possible due to the large amounts of data. The 2D images, both the 2D-C and 2D-P, showed two characteristic image and spectra types, similar to those noted by the FSSP. Figures 28-31 show representative 2D-P and 2D-C spectra from both regions in the cloud closer to the barrier than 30 km and further west. Again, an active and inactive spectra type emerge, the active distinguished on both 2D-P and 2D-C by an increase in numbers in individual bins as well as by broadened spectra. At lower levels in the cloud, at 60 kPa and below, the 2D-C spectra show that the distribution of cloud particles within the total cloud has become essentially uniform: differences between active and inactive spectra are nearly indetectable. 2D-P probe spectra, however, indicate a difference between active and inactive regions at all levels sampled. At all levels in the cloud,

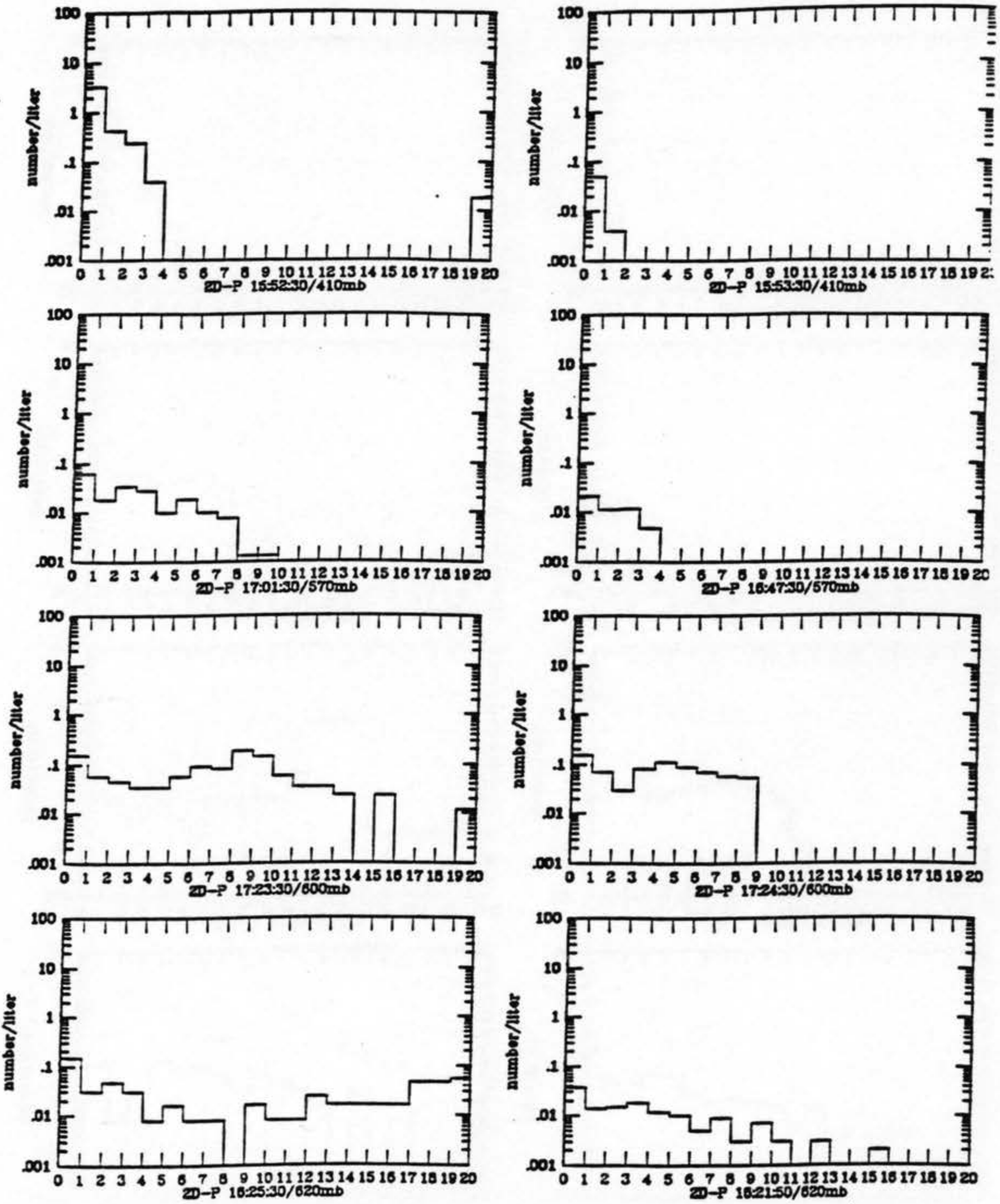

Figure 28: 2D-P data. 28 November. All spectra are taken from greater than 30km west of the barrier. Pressure height and time are indicated below each spectrum, while bin numbers are in 200 μm increments. Left hand column represents 'active' spectra, right hand column represents 'inactive' spectra. All times UTC.

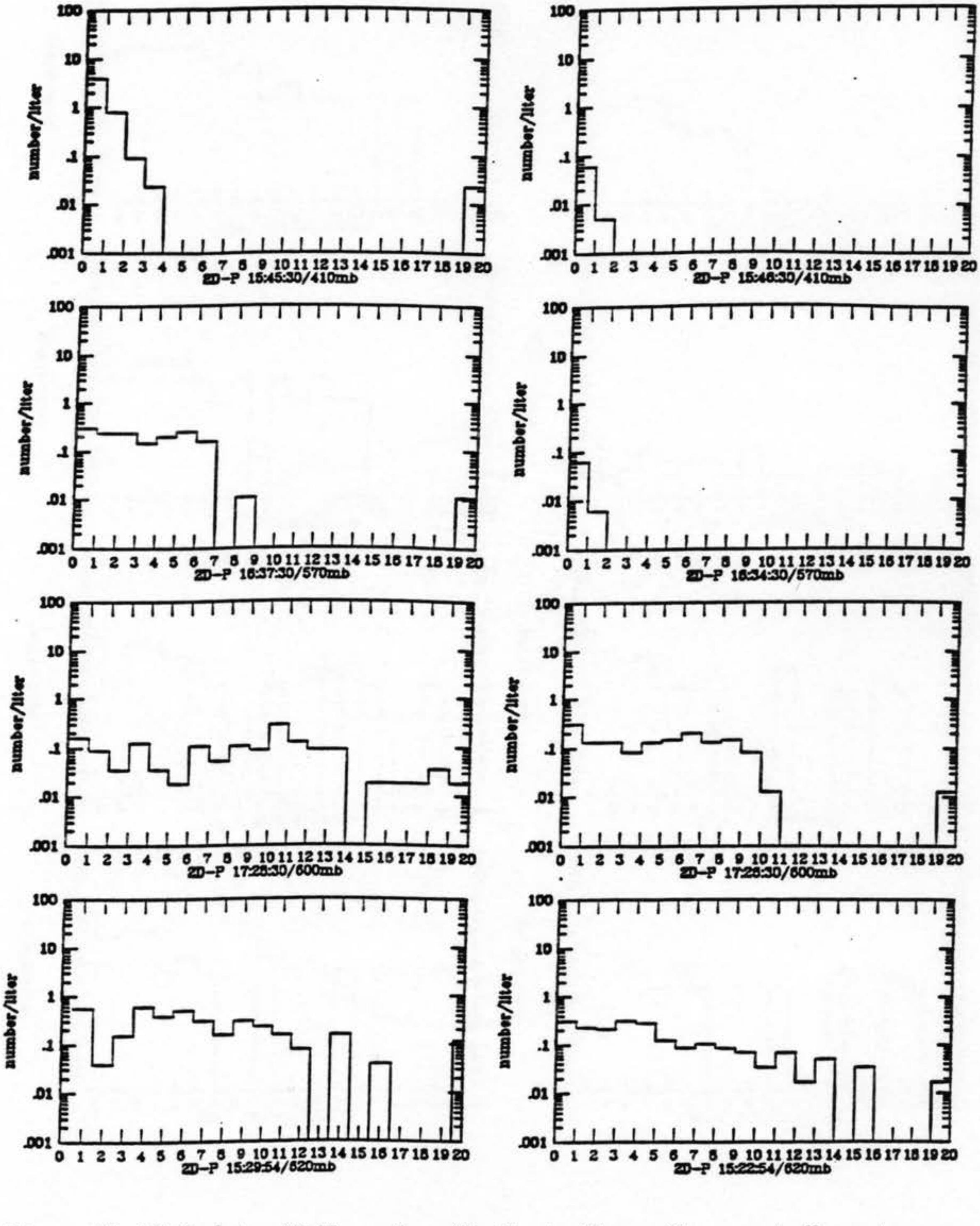

Figure 29: 2D-P data. 28 November. Similar to Figure 28, except all spectra are taken from less than 30km west of the barrier.

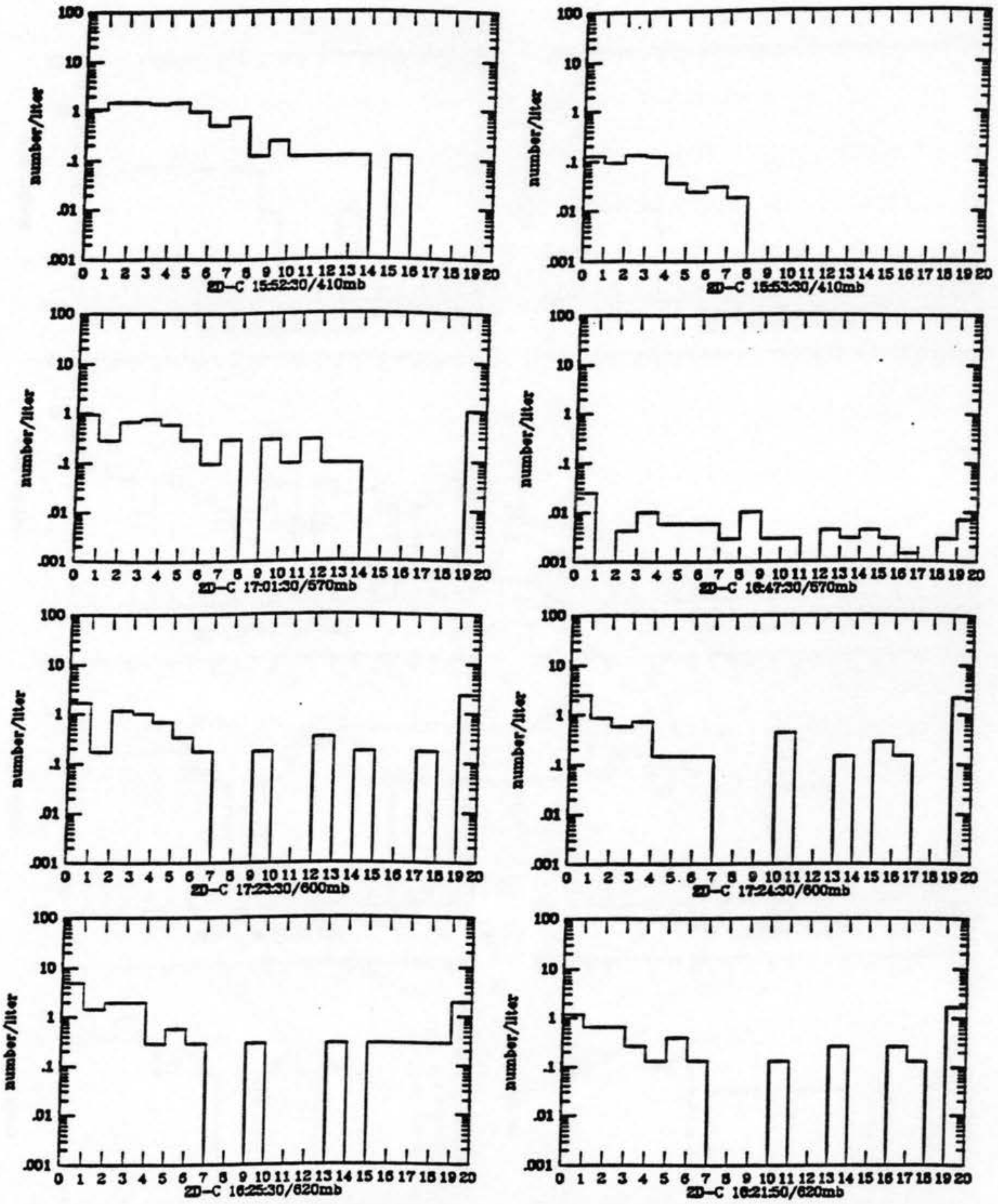

Figure 30: 2D-C data. 28 November. All spectra are taken from greater than 30km west of the barrier. Pressure height and time are indicated below each spectrum, while bin numbers are in 50 μm increments. Left hand column represents 'active' spectra, right hand column represents 'inactive' spectra. All times UTC.

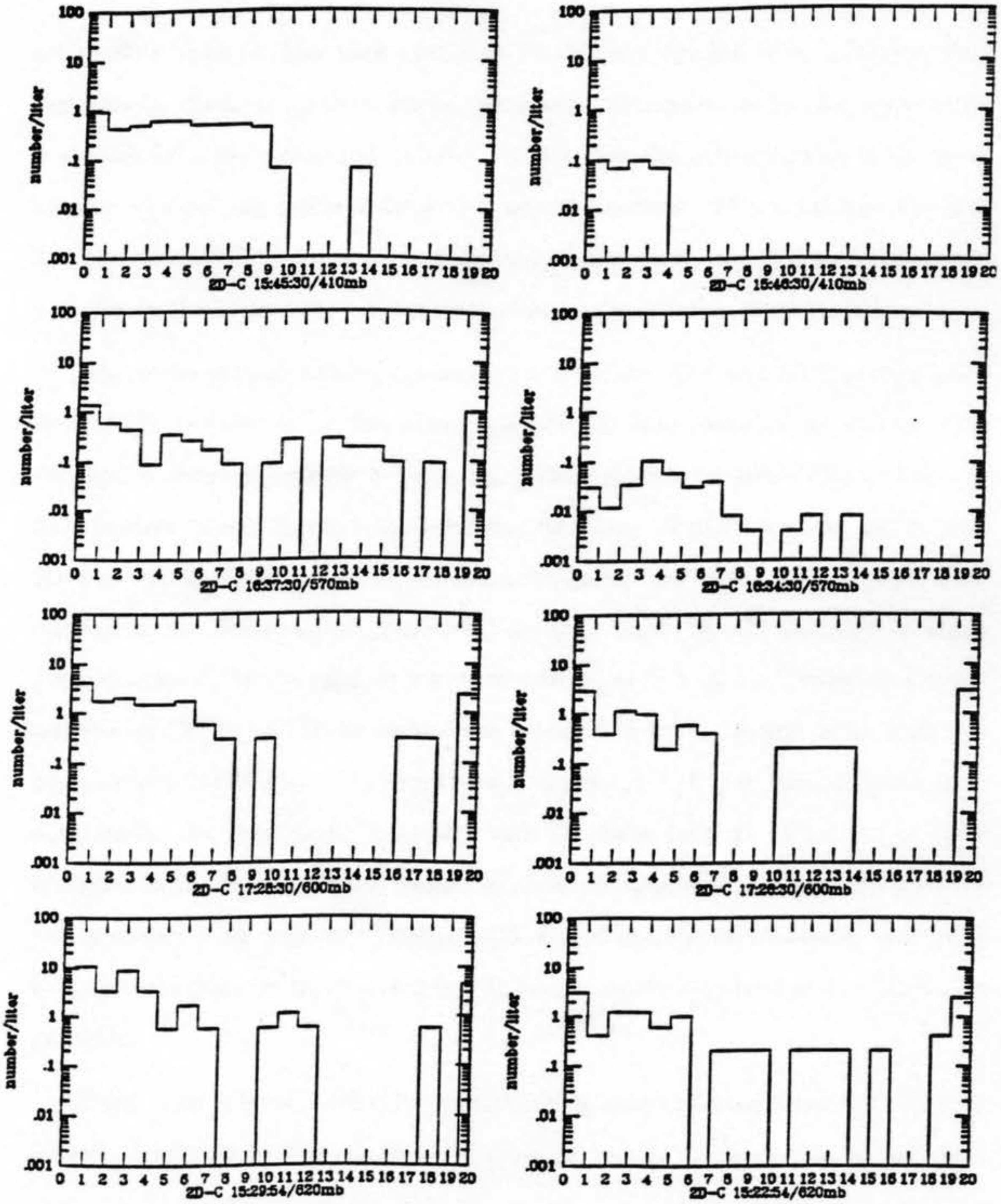

Figure 31: 2D-C data. 28 November. Similar to Figure 30 except all spectra are taken from less than 30km west of the barrier.

active 2D-P spectra show both increased number concentrations in individual bins and broader spectra. At lower levels, the number concentration in the smaller bins is similar for both active and inactive regions, but the active regions show much broader spectra, indicative of larger ice particles present. This is because the first five bins in the 2D-P size spectra represent smaller sizes, or cloud particles, while particles in the larger bins are representative of precipitation-sized particles.

Time series of total number concentration from the 2D-P and 2D-C probes taken west of the barrier reveal that cloud and precipitation particles, as well as SLW droplets, undergo a periodic cycle as the aircraft travels perpendicular to the barrier. Figures 32 and 33 show the total concentrations of SLW droplets, 2D-P, and 2D-C as well as liquid water content calculated from FSSP data. The 2D-probe concentrations are closely linked, and reveal apparent bands or cells that vary in width from less than 6 km to near 30 km, with spacing of 5 to 20 km (using an average airspeed of 100 m/s). These widths and separations are consistent with what was estimated by radar data. The liquid water content and droplet concentration data show similar features, mostly colocated with 2D-probe data. In all but two or three instances in the figures shown, regions of elevated cloud and precipitation particles are colocated with regions of higher SLW and droplet concentrations, indicating that active regions for SLW correspond to active regions for cloud and precipitation particles.

There is an inherent difficulty in comparing data collected from two different frames of reference. The radar is Eularian in nature, whereas the aircraft data are lagrangian. With a fixed, vertically-pointing radar at the base of the barrier, the observer is left without information about the orographic cloud prior to the time that it passes overhead. There simply is no radar record of the genesis and early life of the enhanced-reflectivity elements. Similarly, an aircraft can sample

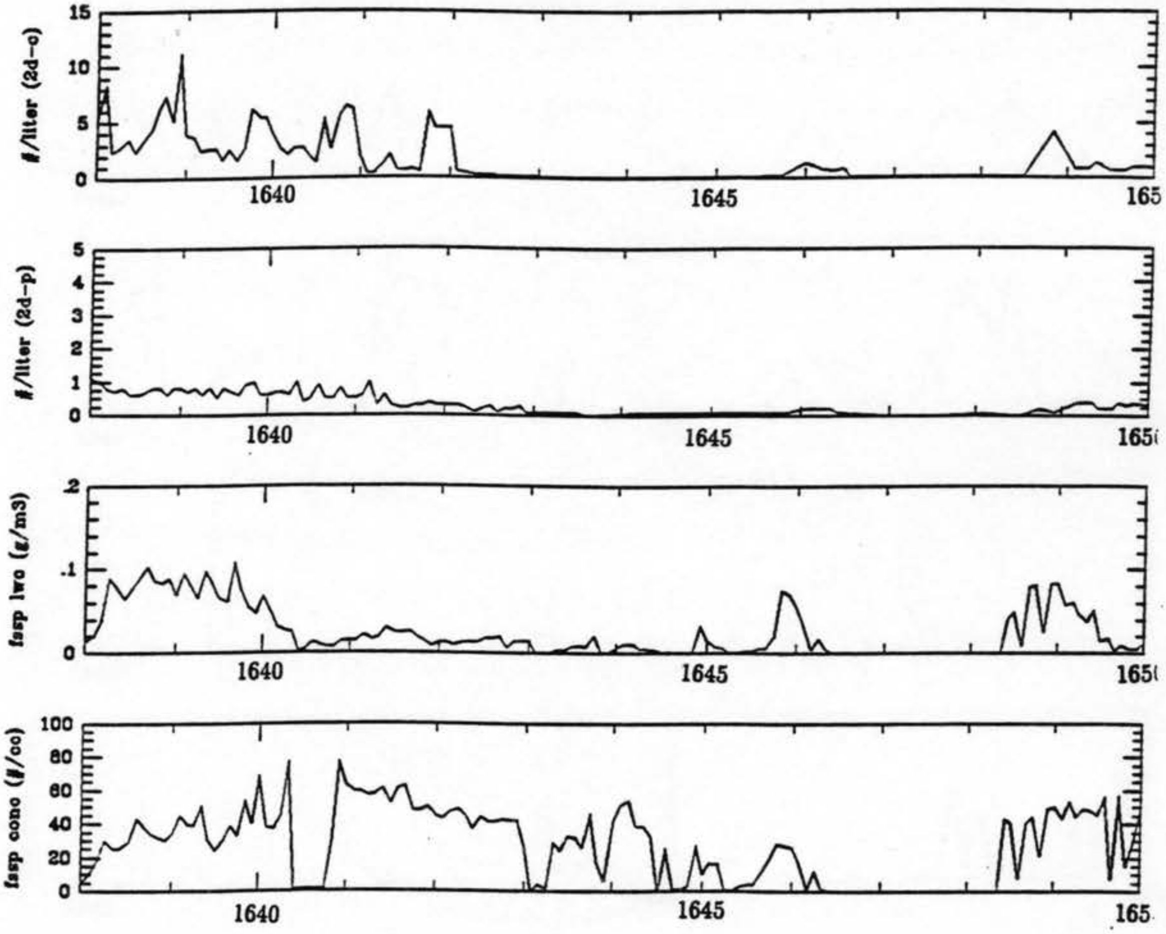

Figure 32: Time series of cloud and precipitation particle concentrations, as well as lwc and SLW concentration for level flight leg at 6650 meters msl (57 kPa) between 1638-1650 UTC 28 Nov. At 1638 the aircraft is at or near the barrier, moving to 55km west by 1650.

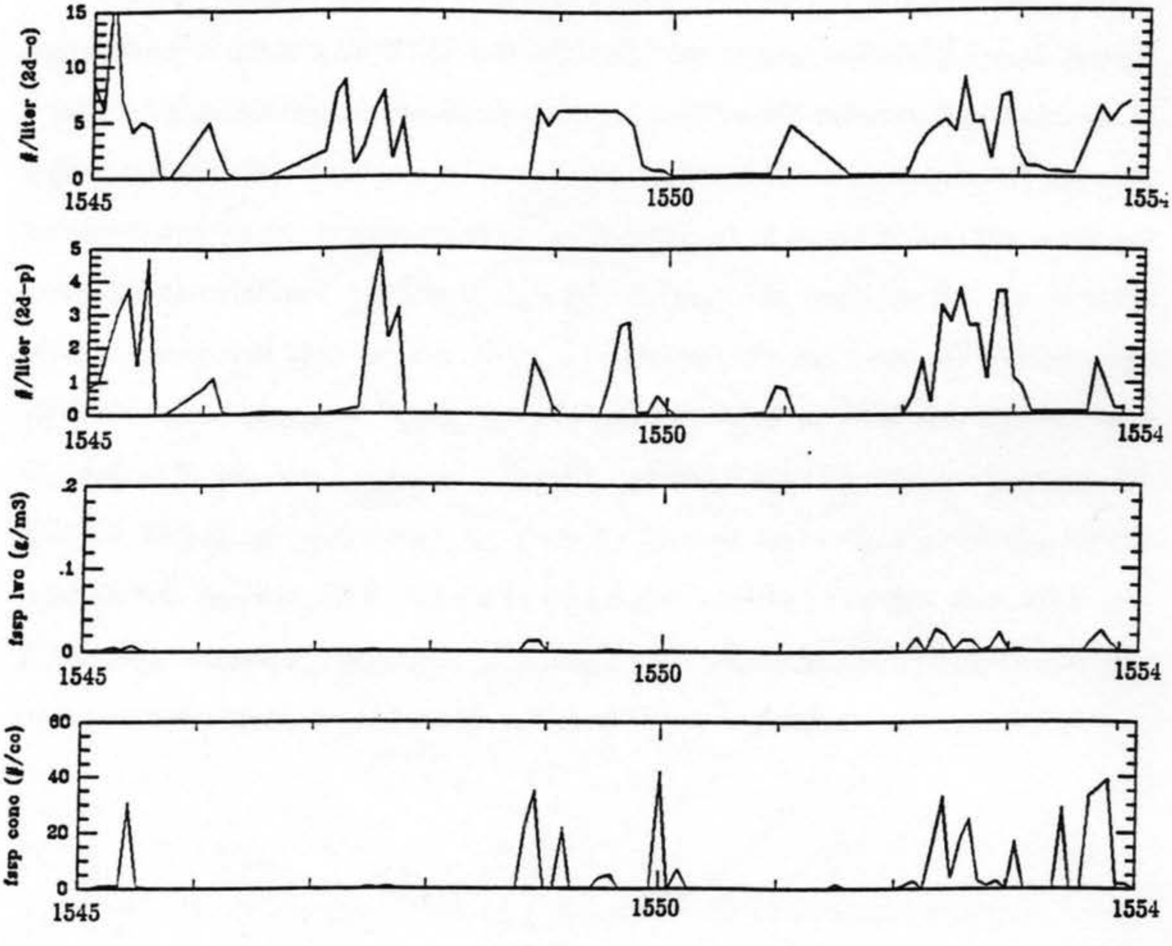

Figure 33: Time series of cloud and precipitation particle concentrations, as well as lwc and SLW concentration for level flight leg at 9000 meters msl (41 kPa) between 1545-1554 UTC 28 Nov. At 1545 the aircraft is at or near the barrier, moving to 50 km west by 1554.

only a small parcel of the total cloud at a single time. Uttal avoided this problem by assuming the orographic cloud to be steady-state. In the present study it would appear that within what has been formerly called a stable orographic cloud, there are transient features superimposed upon an essentially steady-state orographic process. Furthermore, the fact that the FSSP data were collected in one-minute bins makes comparison to 2D-P and 2D-C data difficult. Ice crystal and droplet size spectra appear to undergo similar variations, but the relationship between liquid and ice at a given point in the cloud is a relationship that, given the current dataset, can only be speculated upon. It appears that 'active' regions of liquid within the cloud are located in association with 'active' regions of ice particles, implying that the physical process involved at that location (enhanced vertical motion, perhaps) is responsible for both condensation of liquid and solid particle growth. It is also possible that the active liquid size spectra are slightly out of phase with the ice particle size spectra, as per the arguments put forth by Rauber and others pertaining to the relationship between SLW and ice in orographic clouds. The fact that 2D-P and 2D-C data comprise a 'snapshot' of a single time while the FSSP data is averaged over a one-minute span makes this a difficult issue to resolve.

7. RADIOMETER DATA

The relationship between vapor, liquid and ice is described by Uttal *et al.* (1988) as being dependent on updrafts and downdrafts within the orographic cloud. Vapor will be depleted by condensation and deposition in regions of updraft, while evaporation and sublimation in regions of downdraft will increase vapor amounts in the cloud. Supercooled liquid droplets will form as vapor condenses, but will be depleted by accretional growth on ice crystals and by evaporation. Ice is a sink term in the liquid interaction, as in the region of the barrier ice is removed from the cloud by precipitation. A number of authors have commented on the inverse relationship between SLW and precipitation intensity in orographic clouds (Rauber and Grant 1986, Sassen 1987, Sassen *et al.* 1990, and Reynolds and Kuciauskas 1988). It has been noted that during times of higher intensity precipitation, ice crystals will remove SLW from the cloud by accretion, while during light or no snowfall SLW is able to accumulate within the cloud.

As has been previously noted, the dual-channel radiometer returns a value for path-integrated vapor and SLW amounts at one minute intervals within the cloud while in the vertically-pointing mode. A determination of path-integrated ice depth would make possible an intercomparison of the three phases of water within the orographic cloud, perhaps shedding some light on the relationships therein. Sassen (1984) derives an equation for determination of ice content W (gm^{-3}) from the radar reflectivity factor Z ($\mathrm{mm}^6\ \mathrm{m}^{-3}$) for a vertically-pointing Ku-band radar. Using data from polar regions for column, bullet and side-planed crystals (Sato *et al.* 1981; Kikuchi *et al.* 1982), the relationship between W and Z was found to be $W = 0.037Z^{0.629}$. Integration of this equation through the atmosphere returns a water-equivalent ice column depth, which can be used for contrast with the vertically-pointing radiometer data. Sassen points out that this equation is valid only for low reflectivity values such as those found in orographic clouds. This relationship would result in significant overestimation of ice content if used with higher reflectivity values. For the current case, it must be kept in mind that because of the limitations in these kind of derivations, as well as the uncertainty in reflectivy due to processing uncertainties mentioned earlier, that the value for path-integrated ice depth should be used in a qualitative and not a quantitative sense.

Using the equation derived by Sassen, the reflectivity values from the CSU Ku-band radar were converted to an integrated ice depth for comparing/contrasting with the radiometer data. Figure 34 shows the path-integrated signals for vapor, liquid, and ice for the period 28 November 1200 UTC - 29 November 0000 UTC. It can be seen that the greatest ice depths occur during the time 1500-1530 UTC on the 28th. This corresponds with the period of highest snowfall intensity as noted by observers at the radar site, and corresponds to trough passage. SLW is low (where data are present), with the exception of a small spike just prior to 1400 UTC. Afterwards, SLW depths are all below 0.1 mm.

Figures 35 and 36 represent the time period between 0000 UTC and 1330 UTC on the 29th. This data record is uninterrupted. Snowfall records indicate that there was precipitation at the radar through 0500 UTC on the 29th, with a period of light to no snowfall until 0700 UTC, after which there was consistently light snowfall through 1200 UTC. The highest SLW values for the entire storm period are found between 0400-0700 UTC on the 29th, corresponding to the period of diminished intensity of snowfall. However, during the period 0700-1400 UTC on the 29th, it can be seen that there are periods where localized maxima in SLW depth are coincident with ice depth maxima. Good examples are the periods 0730-0800 UTC and 0830-0900 UTC 29 November, where ice and SLW both exhibit local maxima.

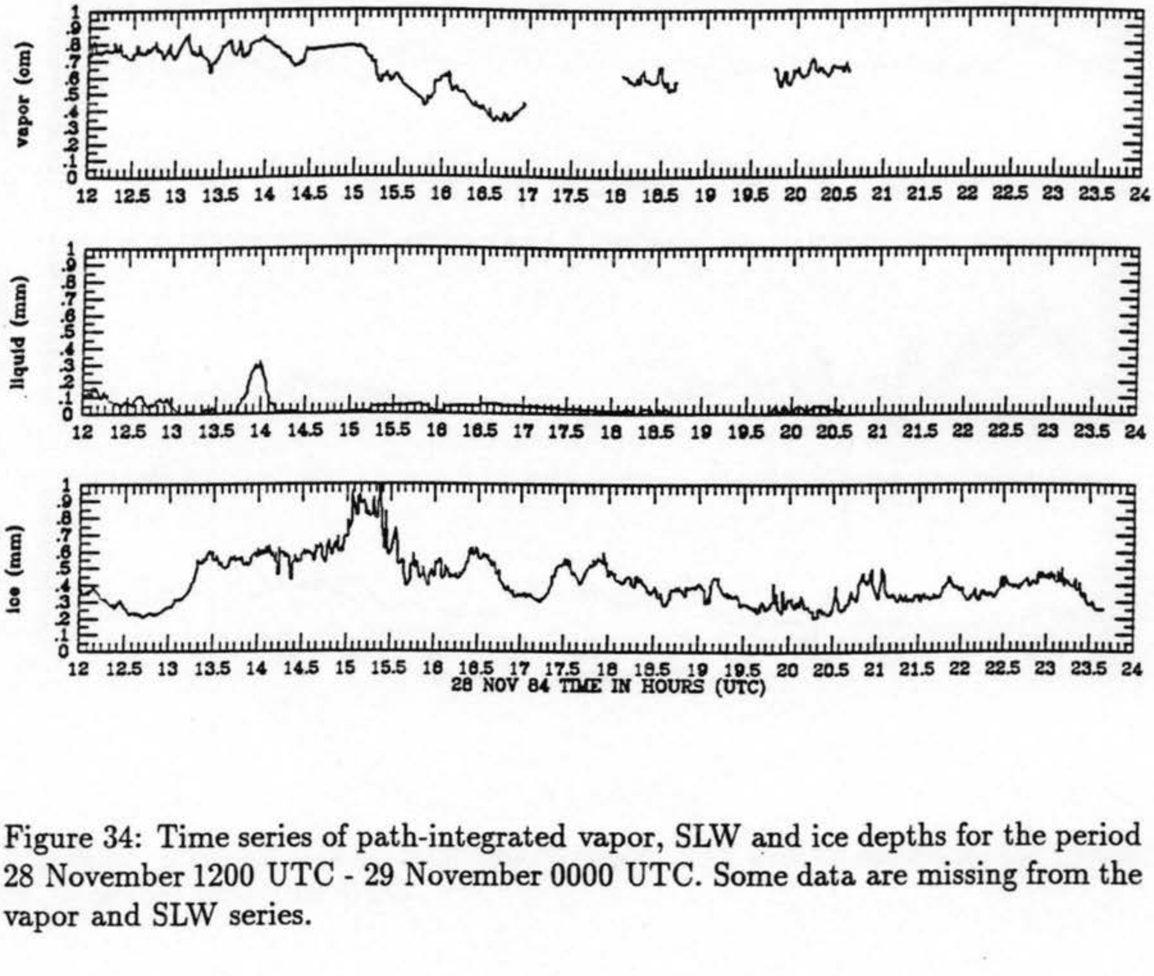

Figure 34: Time series of path-integrated vapor, SLW and ice depths for the period 28 November 1200 UTC - 29 November 0000 UTC. Some data are missing from the vapor and SLW series.

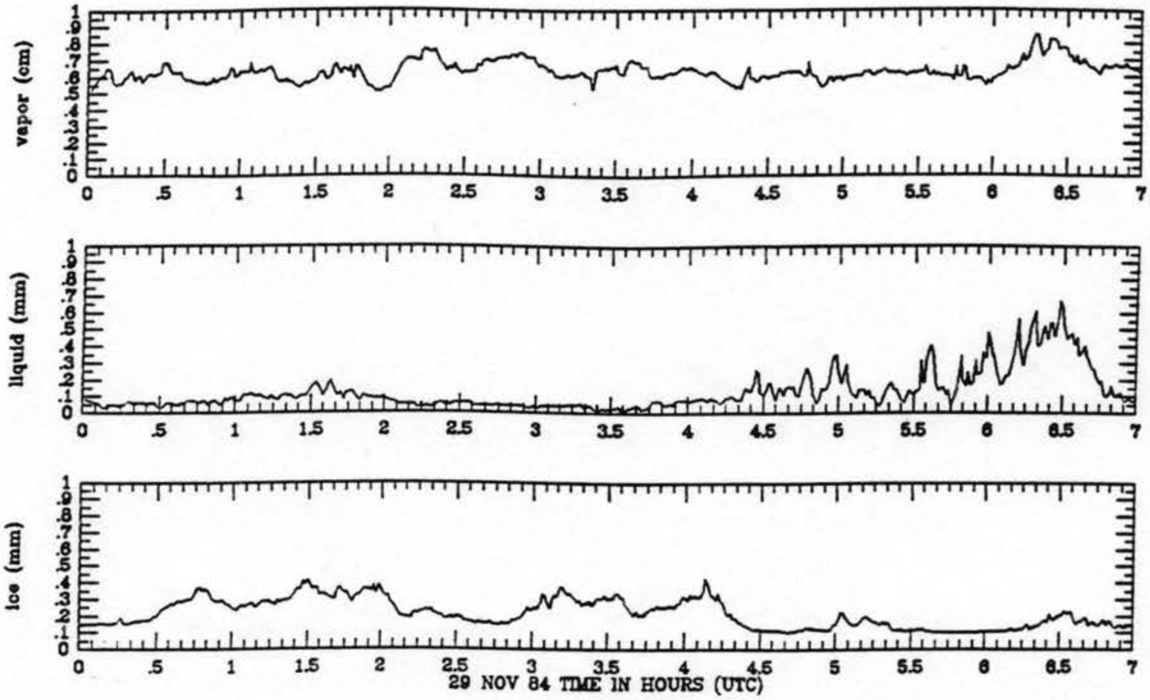

Figure 35: Time series of path-integrated vapor, SLW and ice depths for the period 29 November 0000-0700 UTC.

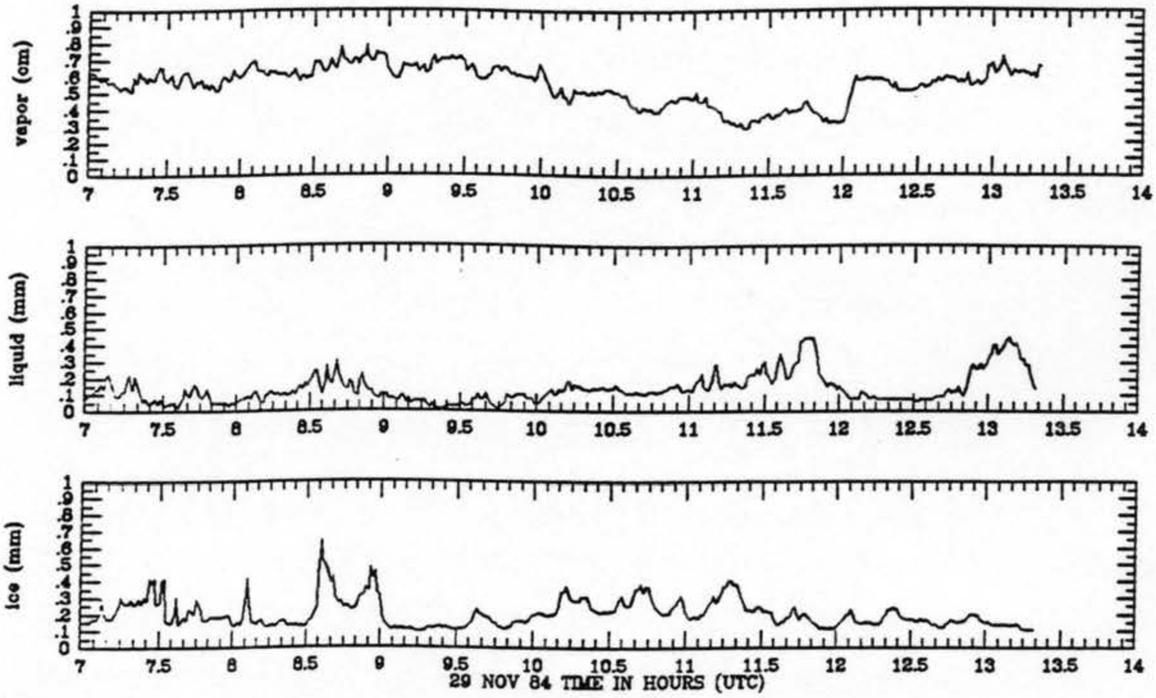

Figure 36: Time series of path-integrated vapor, SLW and ice depths for the period 29 November 0700-1400 UTC.

In the following section, statistical techniques will be employed in an effort to determine whether some of the cyclical features, which can be seen both in radiometer data and radar reflectivity plots, can be elucidated further.

8. STATISTICS AND SPECTRAL ANALYSIS

The time series of vapor, SLW and ice depth (Figures 34-36) give an indication of having a cyclical component. Vapor maintains a fairly steady depth, having maximum values near 0.8 cm and minimun values near 0.3 cm total depth, with an average near .6 cm. A cyclical or sinusoidal component can be seen in this vapor signal, the most prominent period being at approximately 60 minutes. Superimposed upon this cycle is a variation at greater frequency, with a period apparently around 15-20 minutes. Integrated SLW depth, while not as obviously cyclic as vapor, still gives an indication of having a repetitive component. Large peaks, such as those at 0630, 0830 and 1145 UTC do not appear regular in nature, but superimposed upon these larger peaks is a possibly repetitive sequence of smaller peaks and valleys. This smaller sequence has a period of around 30 minutes. Ice column depth is similar to liquid, in that there appears to be a long-term cycle of approximately 80 minutes, with a smaller cycle superimposed upon it.

As an aid to investigation of the sinusoidal nature of the vapor, SLW and ice column depths, statistical analysis of the three time series was performed. Due to the incomplete data prior to 0000 UTC 29 November, time series analysis was performed only on data between 0000-1300 UTC on the 29th. Autocorrelation, spectral analysis, and cospectral analysis are all techniques that may give some insight into the nature of the cycles, and thus help in understanding the interrelationships between the various phases of water in an orographic cloud. However, keeping in mind that statistical analyses are designed for stationary time series and in a real orographic cloud processes are always in a state of flux, there will be some ambiguity which may obscure any conclusions about the relationships between the various phases of water in an orographic cloud and the physics involved.

Following Panofsky and Brier (1958), the autocorrelation of each of the fields was found. The autocorrelation is basically a linear correlation coefficient between a given time series and the same time series an interval of time later. Figure 37 shows the autocorrelogram for the data from 0000-1300 UTC 29 November 1984. The vapor autocorrelogram shows an enhanced correlation at periods of around 30, 60, and 90 minutes. These could be individual cycles, or the latter two could be harmonics of the first. Liquid and ice do not show as coherent a signal, but both do show a small peak in autocorrelation near 30 minutes. The liquid autocorrelogram shows another peak at 85 minutes, while the ice autocorrelogram indicates peaks at 65 and 90 minutes.

Analysis of spectral density can help in drawing out periodic relationships from time series as well. Spectrum analysis is a statistical application of harmonic analysis schemes to the autocorrelation functions of a time series, which will determine the amount of variance contributed to the total variance by oscillations at different frequencies. Seigel (1977) and Ciesielski (1980) used spectrum analysis as an aid in investigating the 21-26 day oscillation in Pacific Ocean sea-surface temperatures, and the techniques applied there were adopted for the current case. The spectral densities of vapor, SLW and ice are shown in Figure 38. The vapor spectral density shows a strong contribution to the total variance at a frequency of 0.0005 $\sec^{-1}$ with a lesser contribution at 0.001 $\sec^{-1}$. These two frequencies translate to periods of 33 and 17 minutes, respectively. The spectral density function for liquid does not show as strong a signal as vapor does. However, there can be seen small peaks at frequencies of 0.0009 $\sec^{-1}$, 0.00055 $\sec^{-1}$, and 0.00035 $\sec^{-1}$, or 18.5, 30, and 48 minutes. Spectrum analysis of the derived ice column depth indicates that it is similar to the liquid series, in that a single dominant spike is not present in the spectral density plot. Instead there are smaller peaks at frequencies of 0.0008,

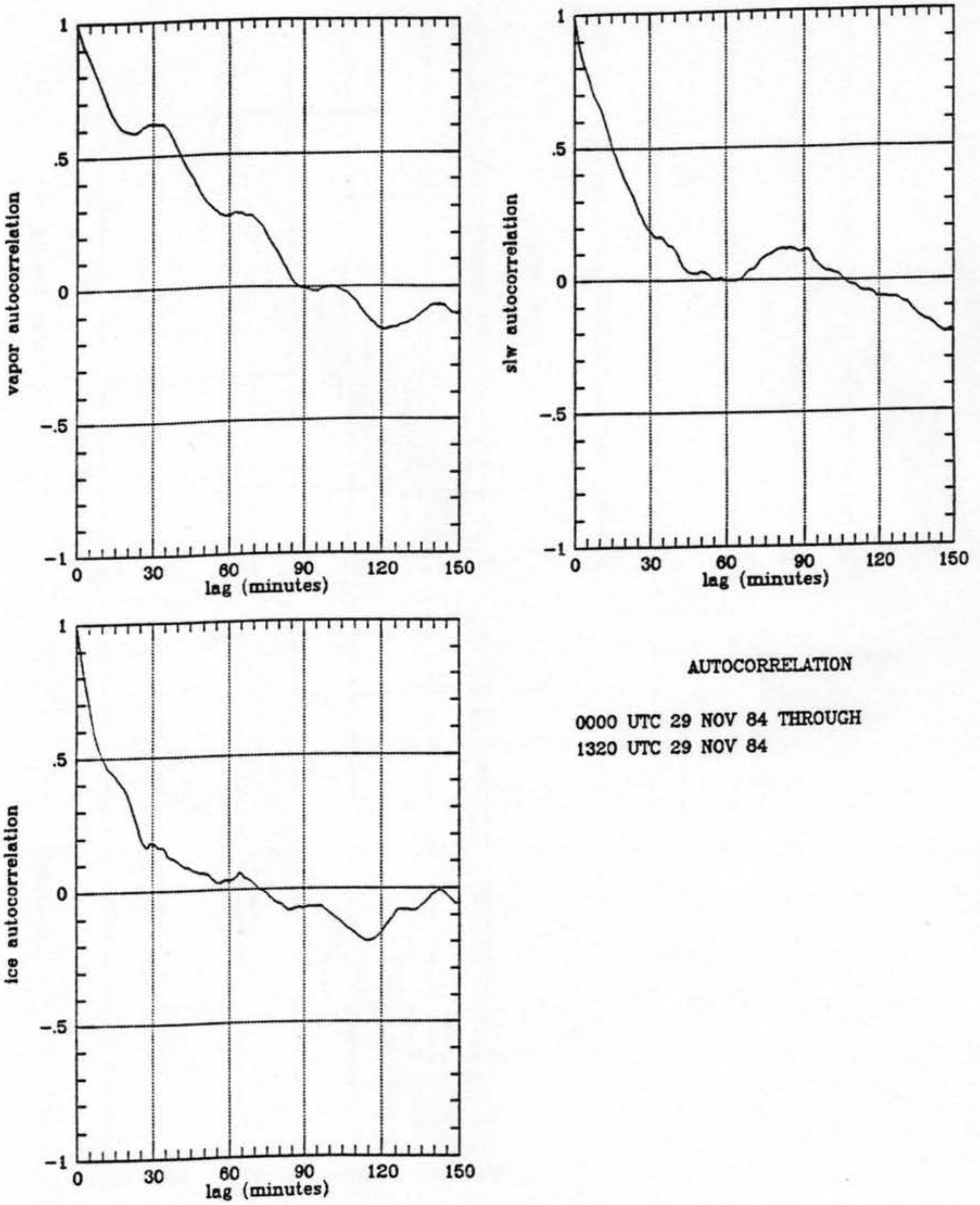

AUTOCORRELATION

0000 UTC 29 NOV 84 THROUGH
1320 UTC 29 NOV 84

Figure 37: Autocorrelation of vapor, SLW and ice depths. Data are from 0000-1320 UTC 29 November.

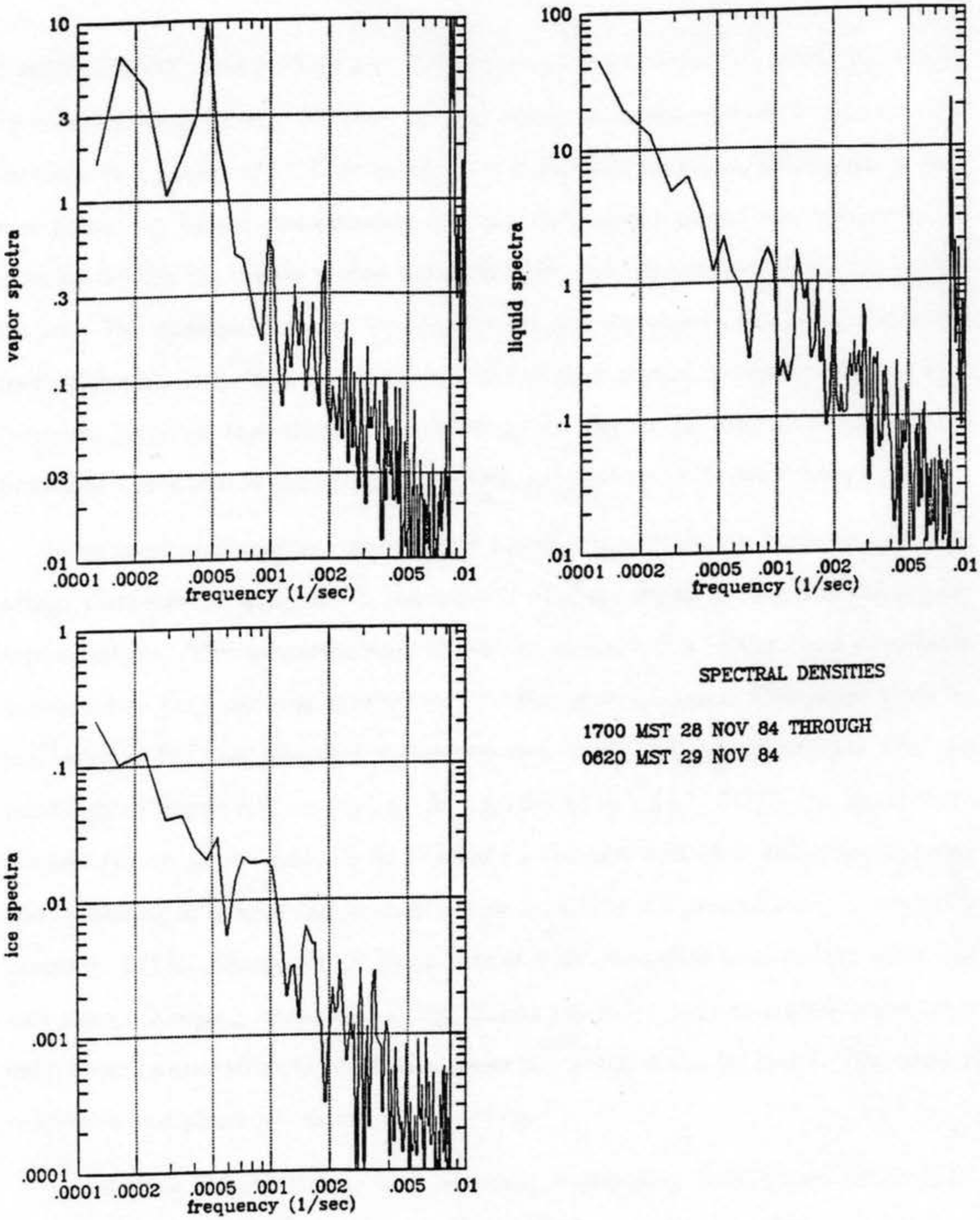

SPECTRAL DENSITIES

1700 MST 28 NOV 84 THROUGH
0620 MST 29 NOV 84

Figure 38: Spectral densities for vapor, SLW and ice. Time series is between 0000-1320 UTC 29 November.

0.00055, 0.00035, and 0.00022 $\sec^{-1}$. These correspond to periods of 21, 30, 48 and 76 minutes, respectively. All three spectra show an increased contribution to total variance at a period of 17-21 minutes, as well as 30-35 minutes. This longer period was picked up by the autocorrelogram, but the shorter period was not revealed, likewise for the 48 minute period noted in SLW and ice and the 76 minute period for ice. The question remains whether or not the increased contribution at these frequencies is a real effect or a harmonic of a shorter period oscillation. There is no question, however, that there is a definite periodicity to the time series of all three phases of water within the orographic cloud sampled on 28-29 November 1984.

Cross spectrum analysis can be used to test the correlation between two time series. Cospectrum, quadrature, coherence and phase are all products of cross spectrum analysis. The cospectrum measures the contribution to the total covariance between two time series of oscillations at different frequencies. The phase gives an indication of the relationship between two time series in terms of whether they are positively or negatively correlated. As mentioned in Seigel (1977), the significance of cross spectrum analysis can be clouded by the fact that each individual time series contains persistence and/or autocorrelations. For the present study a computer program, ISTAT, developed by Paul Hein at CSU, was used to calculate coherence and phase. Keeping in mind that the results are to be used in a qualitative sense only, some relationships between the cycles noted above can be found. The plots of coherence and phase are shown in Figure 39.

Vapor does not appear to have a strong relationship with either ice or SLW, based on the coherence calculations. The significance is below 50% for periods of more than 10 minutes, indicating that any apparent correlation is just as likely to be accidental as it is to be real. This is not surprising in light of the fact that the integrated vapor depth is an order of magnitude higher than the integrated depths

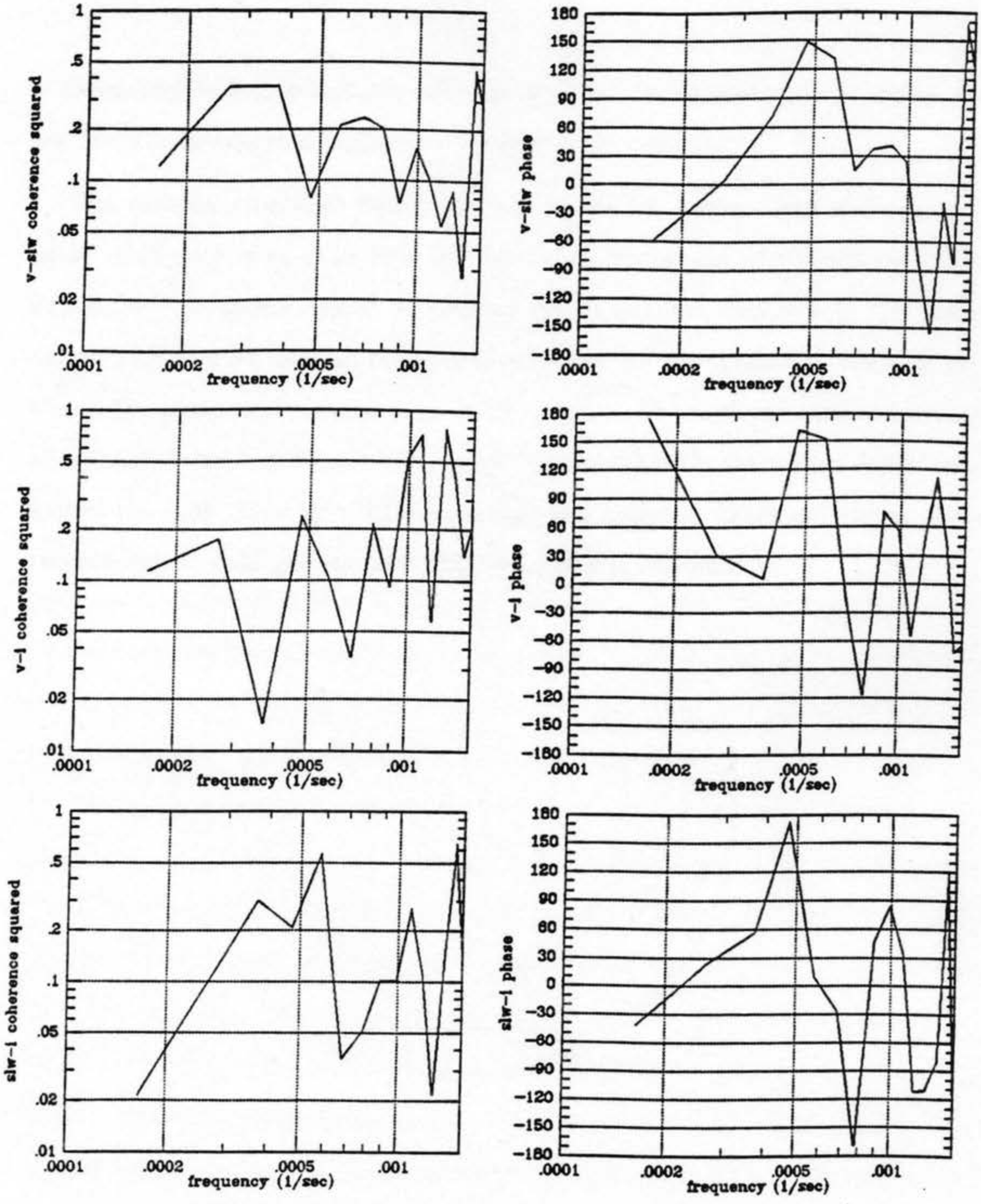

Figure 39: Coherence squared (left) and Phase (right) for vapor vs. SLW (v-slw), vapor vs. ice (v-i) and SLW vs. ice (slw-i). Time series data are from 0000-1320 UTC 29 November.

of either SLW or ice, so that any effect of variations in the latter two quantities are not likely to be reflected in the total column vapor amount.

The coherence between liquid and ice (Figure 39, bottom left) indicates two peaks of slightly more than 50% significance at frequencies of 0.00058 sec^{-1} and 0.0015 sec^{-1}, or approximately 29 minutes and 11 minutes, respectively. The phase diagram (Figure 39, bottom right) indicates that the two quantities are in phase, that is the phase angle is near zero, at 29 minutes. At the eleven minute peak the phase angle is between 90 and 120°, which indicates that the ice column depth trend follows the SLW trend by a little more than two minutes. While not strong, these two coherence peaks give an indication of a possible relationship.

9. DISCUSSION

Banded convection, both embedded and as a separate cloud entity, has been studied by a number of authors in a variety of situations. Release of potential instability, gravity waves, and Conditional Slantwise Instability have all been mentioned as possible physical mechanisms responsible for generating banded precipitation. While a single case makes ascertaining the generating mechanism for the presumed bands in the Park Range an daunting task, it is possible to address several of these other mechanisms and discuss their applicability to the present situation

Conditional Slantwise Instability (CSI) has been discussed both theoretically (Bennets and Hoskins 1979; Bennets and Sharp 1982) and observationally (Byrd 1988; Emanual 1988) as a mechanism responsible for precipitation bands. Release of latent heat has been seen to provide for an unstable atmosphere even where the atmosphere may be stable to unsaturated displacements. The main criteria for CSI, according to Bennetts and Hoskins, is that the horizontal temperature gradient be large and the Richardson Number large. Bands form in a variety of orientations relative to midlatitude cyclones where motion is ascribed to have been along surfaces of constant 'absolute momentum', defined as: $M \equiv v_g + fx$, where v_g is the geostrophic flow in the direction of the thermal wind, x is a coordinate in the direction of the temperature gradient and f is the Coriolis parameter (Emanual, 1988). Emanual describes a case from the east coast of the U.S. where sounding data showed the atmosphere to be essentially stable, while an aircraft track along a surface of constant M indicated that the atmosphere was neutral to slightly unstable. All authors report on precipitation bands with a size dimension on the order of 100 km spacing, with much larger lengths. Time scales have been mentioned as being on the order of days, making it unlikely that CSI is a factor for the present case.

Rasmussen *et al.* (1993) discuss a situation from the Colorado front range from 15 November 1987 where forced ascent over a cold front released potential instability resulting in banded convective precipitation. In that case, sounding data indicated that the atmosphere was potentially unstable above the front, resulting in snowbands being formed behind the leading edge of the front as it propagated southward. For the present case, the atmosphere was seen to be at most neutrally stable for most of the period of interest (Figure 11), with some small regions of potential instability ($d\theta_e/dz < 0$) occurring. In the case of Rasmussen *et al.* the Denver sounding showed that the lapse rate above the frontal surface was dry-adiabatic, implying that the convection there would be considerably more vigorous than any in the Park Range region where the Craig soundings (Figures 13-16) show that at its most unstable the atmosphere becomes moist adiabatic. While it appears that release of latent heat will not be sufficient to drive the embedded convection seen by the Ku-band radar, the fact that the soundings indicate that the atmosphere was neutral to slightly potentially unstable at times, with cold aloft as well, indicates that it is possible that latent heat release could play a factor.

Marwitz (1980) showed a case from the San Juan Mountains in southwestern Colorado where aircraft data revealed gravity waves with a wavelength near 4 km (Figure 3). Since, in Marwitz' case, there was a decoupled layer noted during the storm, it seems possible that perhaps this is a factor in the Park Range as well. Conceptually, what could happen is that as air is deflected upwards over the decoupled layer, there will be a restoring force. A gravity wave would set up along the interface between the decoupled layer and the ambient flow. Using the Brunt-Väisälä frequency $N^2 = \frac{g}{\theta}\ \frac{d\theta}{dz}$ where g is the gravitational acceleration and θ is potential temperature, and using data from the first aircraft flight where the aircraft penetrated the decoupled layer during a missed approach at Hayden, a Brunt-Väisälä frequency of $N = 0.0139\mathrm{sec}^{-1}$ can be calculated. This corresponds to a period ($\tau = \frac{2\pi}{N}$) of approximately 8 minutes, which is significantly shorter than the periods either observed or found from spectral analysis in this case.

Durran and Klemp (1982) discuss a situation where the Brunt-Väisälä frequency is affected by moisture, where a good approximation of the saturated Brunt-Väisälä frequency is given by:

$$N_m^2 = g\left\{ \frac{1 + (Lq_s/RT)}{1 + (\epsilon L^2 q_s/c_p RT^2)} \times \left(\frac{dln\theta}{dz} + \frac{L}{c_p T} \frac{dq_s}{dz} \right) - \frac{dq_w}{dz} \right\}$$

where L is the latent heat of vaporization, q_s is the saturation mixing ratio, q_w is the total water mixing ratio, R is the ideal gas constant for dry air, T is temperature, c_p is the heat capacity of dry air, and $\epsilon = \frac{R}{R_v}$ where R_v is the gas constant for water vapor. Using data from the same aircraft flight, the equation for the moist Brunt-Väisälä frequency returns a value for N of 0.00423 sec^{-1}, or a $\tau = 24.7$ minutes. This is more in line with the values returned both by observations and the spectral analysis. It must be kept in mind, however, that the entire nature of the decoupled layer-free atmosphere interface is not known, and as the current aircraft samples came near the western terminus of the decoupled layer, they must be considered rough estimates.

It would appear, then, that air travelling towards the barrier is influenced by orographic lift due to topography, as well as an additional lift due to the decoupled layer. Since the interface between the ambient flow and the decoupled layer is not a rigid boundary, it is possible for a gravity wave to develop on the interface as air parcels experience the restoring force. Microphysically, the air experiencing additional upward motion compensate with production of additional SLW, which fosters an environment conducive to enhanced crystal growth, with enhanced aggregation probable as well. These areas containing greater numbers and larger ice crystals will be expressed on the radar as areas of increased reflectivity, which propagate towards the radar with the mean flow. Observers on the ground have noted that a common sequence near the barrier is for a period of light snowfall to transition into moderate to heavy snowfall where crystals are both rimed and aggregated, indicating surplus SLW. Snowfall will then become lighter in intensity, with decreased riming and aggregation, until snowfall either stops or becomes light in intensity and dominated by pristine crystals, which would indicate that the observer is at that point between enhanced reflectivity/snowfall bands.

10. RESULTS

It has been shown that embedded within the deep orographic cloud observed in the COSE IV domain during 28-29 November 1984 there are regions of enhanced cloud activity. These regions are manifest as areas of enhanced reflectivity as seen by a vertically pointing Ku-Band radar, with a signature suggesting cells and precipitation streamers as discussed by Marshall and others. Particle data taken from instrumented NCAR aircraft support the presence of what has been here termed active regions of the cloud, in terms of supercooled liquid water production and particle nucleation and/or growth. Both ground-based remote sensing and aircraft data suggest that individual regions have a dimension perpendicular to the barrier of between 5 and 30 km, with similar distances separating individual active regions. The instrument suite in place for COSE IV made it impossible to determine whether these active regions took the form of bands oriented paralled to the barrier or of individual cells. Radar data from a previous COSE experiment suggest that a banded orientation is common, but confirmation that all reflectivity features seen by the radar at the base of the barrier are in the form of bands is impossible at this time. Sounding and aircraft data indicate that throughout the period when the enhanced reflectivity features were seen that a decoupled layer was evident on the windward side of the barrier. Radiometer data indicates that on a large scale, SLW amount within the cloud is inversely related to snowfall intensity, as the largest SLW amounts noted during the event occurred during a period when snowfall was light or nonexistent. It was also noted that smaller SLW maxima occurred coincident with reflectivity maxima, as noted both by surface instruments and aircraft, indicating that SLW production was in excess of SLW depletion by accretion and/or nucleation.

While inconclusive, statistical analyses give an indication of some possible relationships between SLW and integrated ice depth on the order of 11 and 29 minutes. At 11 minutes it appears that the ice maxima follows the SLW maxima, indicating the possibility that SLW is initially produced by updrafts in the cloud, followed by depletion as the SLW is captured by precipitation processes. At the 29 minute peak, the SLW and ice maxima are in phase, indicating that SLW is produced in excess of that scoured out of the cloud by precipitation. It appears, however, that more data are needed to confirm or refute the statistical findings.

Rauber and Grant (1986) proposed a conceptual model of the SLW distribution within a deep orographic cloud, similar to the situation on 28-29 November 1984. In Rauber and Grant's model, SLW exist at cloudtop and near the barrier in the region of maximum orographic lift. Figure 1 (middle), taken from Rauber and Grant, shows that conceptual model. The data from the present case suggest that perhaps some modification of this conceptual model is in order. Figures 32 and 33 reveal the presence of SLW in concentrations $< 0.2gm^{-3}$ at midlevels and upper regions of the cloud as far as 55 km west of the barrier. These regions of SLW have been shown to be positively correlated with regions of higher concentrations of precipitation particles as well. Radar data indicate that regions of higher reflectivity (implying either higher concentrations or greater size of particles or both) advect over the radar continuously during a storm. As the radar was located 10 km west of the barrier, the advection of higher reflectivity over the radar indicates development of the higher reflectivity at distances further to the west than 10 km. Aircraft data (Figures 32 and 33) indicate the presence of SLW and higher precipitation particle amounts as far as 55 km west of the barrier. Peterson *et al.* (1991) developed a conceptual model wherein a blocked or decoupled layer forms windward of the barrier at low levels and can serve to extend the area of maximum orographic lift some distance to the west

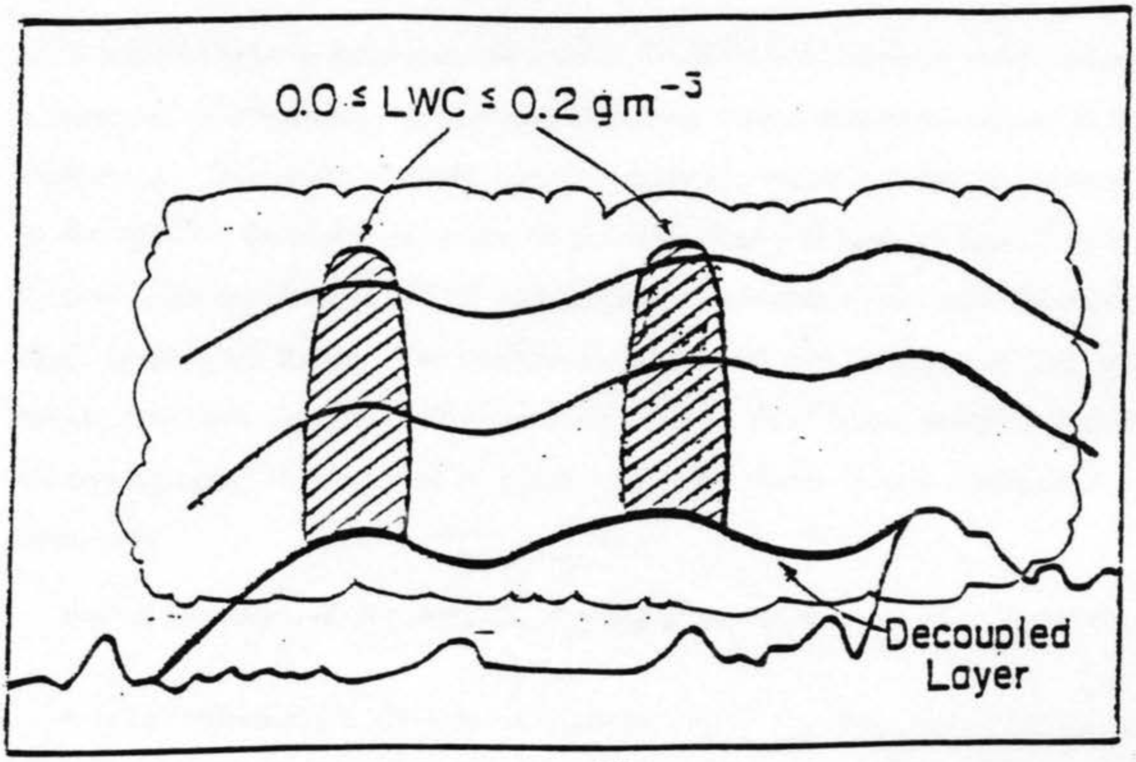

Figure 40: Modified conceptual model of the supercooled water distribution within a deep stratiform Park Range system with cold cloud top. The decoupled layer serves to move the region of maximum lift westward from the barrier. Magnitudes of liquid water contents measured with aircraft are indicated.

of the barrier. As sounding and aircraft data have shown, there was a decoupled layer present on 28-29 November during a considerable amount of the time the storm was active. It is believed that the presence of this decoupled layer is instrumental in the initiation of regions of enhanced SLW and higher particle concentrations at distances well to the west of what was previously anticipated. Figure 40 shows a possible conceptual model of the deep orographic cloud investigated on 28-29 November 1984. The maximum orographic lift is moved to the west by the decoupled layer, which results in the production of SLW at distances well west of the region of maximum topographic lift.

It must be kept in mind that the present case represents a single event and not a summary or climatology of processes occurring within orographic clouds in the Park Range. The depth of cloud, synoptic situation, static stability and presence or absence of a decoupled layer are all processes that will have an impact on the dynamics and distribution of SLW and precipitation within a particular orographic cloud in the Park Range. The analysis of the present case is meant to help gain insight into these processes. More research must be done before conceptual models encompassing all situations in which orographic clouds in this region exist be developed.

during the course of this research, as many questions were raised as answered:

- Is the reflectivity in the form of bands or not?
- What is the morphology of the interface between the decoupled layer and the mean flow?
- What are the implications of the enhanced reflectivity areas to inferences about the nucleation/growth of ice particles within a stably stratified wintertime orographic cloud?

Within what has been called a stably stratified wintertime orographic cloud there now appear transient features that move and oscillate in an interaction with the decoupled layer interface. These features are essential to snowfall in areas windward of the area of maximum orographic lift induced by topography.

11. SUGGESTIONS FOR ADDITIONAL RESEARCH

Further study is needed to throw light upon the dynamical and microphysical nature of the enhanced reflectivity features noted in the previous case. During COSE II, RHI scans from the base of the barrier were taken. The ability to investigate RHI scans from the base of the barrier eastward would give information currently unavailable with a fixed, vertically-pointing radar. It is possible that the radar would be able to detect the boundary between the decoupled layer and the mean flow due to the morphology of the fallstreaks. PPI scans would also make possible a determination of whether the enhanced reflectivity is in the form of bands or not.

In COSE IV, the aircraft was not allowed to make missed approaches at the Steamboat Springs airport, 15 km west of the barrier, nor was it allowed to penetrate the decoupled layer in this region due to FAA imposed minimum enroute altitude restrictions of 4000 m msl as a minimum altitude. The aircraft was allowed to perform missed approaches at the Hayden airport, 55 km to the west of the barrier. This meant that the aircraft could only penetrate the decoupled layer during events when it extended that far westward, and then only at its terminus. The ability to perform missed approaches with an instrumented aircraft at the Steamboat Springs airport would be invaluable, both in terms of gaining information about the boundary between the decoupled layer and the mean flow and information about ice crystal and SLW characteristics in the lower cloud near the barrier.

Finally, the dual-channel radiometer was often left in the vertically-pointing mode when left unattended. This implies that a relatively low-maintenence data source would be to colocate the vertically-pointing Ku-Band radar with the radiometer in the vertical mode and let them gather information for an entire winter season. Again, the data record from COSE II contains this data, as the radiometer at this time was not able to scan. The resultant record would give a researcher an uninterrupted record of path-integrated vapor, liquid and ice depths, and make possible further spectral analysis with a larger dataset.

REFERENCES

Battan, L.J., 1973: Radar Observation of the Atmosphere. University of Chicago Press, Chicago, 324 pp.

Bennetts, D.A., and B.J. Hoskins, 1979: Conditional Symmetric Instability - A Possible Explanation for Frontal Rainbands. *Quarterly Journal of the Royal Meteorological Society*, Vol. 105, 945-962.

Bennetts, D.A., and J.C. Sharp, 1982: The Relevance of Conditional Symmetric Instability to the Prediction of Mesoscale Frontal Rainbands. *Quarterly Journal of the Royal Meteorological Society*, Vol. 108, 595-602.

Byrd, G.P., 1989: A Composite Analysis of Winter Season Overrunning Precipitation Bands over the Southern Plains of the United States. *Journal of the Atmospheric Sciences*, Vol 46, No. 8, pp 1119-1132.

Ciesielski, P.E., 1980. Variability Within the Ocean-Atmospheric System Over the North Pacific. *Colorado State University, Environmental Research Paper No. 25*, 41 pp.

Cooper, W.A, and C.P.R. Saunders, 1980: Winter Storms over the San Juan Mountains. Part II: Microphysical Processes. *Journal of Applied Meteorology*, Vol. 19, No. 8, 927-941.

Douglas, R.H., K.L.S. Gunn, and J.S. Marshall, 1957: Pattern in the Vertical of Snow Generation. *Journal of Meteorology*, Vol. 14, No. 2, 95-114.

Durran, D.R., and J.B. Klemp, 1982: On the Effects of Moisture on the Brunt-Väisälä Frequency. *Journal of the Atmospheric Sciences*, Vol. 39, No. 10, 2152-2158.

Emanual, K.A., 1988: Observational Evidence of Slantwise Convective Adjustment. *Monthly Weather Review*, Vol. 116, Sep. 1988, pp 1805-1816.

Greeson, J.S., D.R. Cobb, L.O. Grant, and L. Lilie, 1979: The Use of the Ku-Band Radar for Weather Modification Research. *Preprints, Seventh Conf. Inadvertent and Planned Weather Modification*, Banff, Amer. Meteor. Soc., 108-109.

Heggli, M.F., L. Vardiman, R.E. Stewart and A. Huggins, 1983: Supercooled Liquid Water and Ice Crystal Distributions Within Sierra Nevada Winter Storms. *Journal of Climate and Applied Meteorology*, Vol. 22, November 1983, 1875-1886.

Hill, G.E., 1992: Further Comparisons of Simultaneous Airborne and Radiometric Measurement Measurements of Supercooled Liquid Water. *Journal of Applied Meteorology*, Vol. 31, April 1992, 397-401.

Hobbs, P.V., and N.T. Funk, 1984: Cloud and Precipitation Studies with a Millimetre-Wave Radar: A Pictorial Overview. *Weather*, Vol. 39, No. 11, 334-339.

Hogg, D.C., F.O. Guiraud, J.B. Snider, M.T. Decker, and E.R. Westwater, 1983: A Steerable Dual-Channel Microwave Radiometer for Measurement of Water Vapor and Liquid in the Troposphere. *Journal of Climate and Applied Meteorology*, Vol. 22, May 1983, 789-806.

Kikuchi, A., S. Tsuboya, N. Sato, Y. Asuma, T. Takeda, and Y. Fujiyoshi, 1982: Observation of Wintertime Clouds and Precipitation in the Arctic Canada (POLEX-North). *Journal of the Meteorological Society of Japan*, Vol. 60, No. 6, 1215-1225.

Long, A.B, B.A. Campistron and A.W. Huggins, 1990: Investigations of a Winter Mountain Storm in Utah, Part I: Synoptic Analyses, Mesoscale Kinematics, and Water Release Rates. *Journal of the Atmospheric Sciences*, Vol. 47, No. 11, 1302-1322.

Ludlam, F.H., 1956: The Forms of Ice Clouds: II. *Quarterly Journal of the Royal Meteorological Society*, Vol. 82, No. 353, 257-265.

Marshall, J.S., 1953: Precipitation Trajectories and Patterns. *Journal of Meteorology*, Vol. 10, Feb. 1953, 25-29.

Martner, B.E., D.B. Weurtz, B.B. Stankov, R.G. Strauch, and E.R. Westwater, 1993: An Evaluation of Wind Profiler, RASS, and Microwave Radiometer Performance. *Bulletin of the American Meteorological Society*, April 1993.

Marwitz, J.D., 1980: Winter Storms over the San Juan Mountains. Part I: Dynamical Processes. *Journal of Applied Meteorology*, Vol. 19, No. 8, 913-926.

Panofsky, H.A. and G.W. Brier, 1958: Some Applications of Statistics to Meteorology. *Pennsylvania State University Press*, 224 pp.

Peterson, T.C., L.O. Grant, W.R. Cotton, and D.C. Rogers, 1991: The Effect of Decoupled Low-Level Flow on Winter Orographic Clouds and Precipitation in the Yampa River Valley. *Journal of Applied Meteorology*, Vol. 30, No. 3, 368-386.

Rasmussen, R.M., A. Crook, and C. Kessinger, 1993: Snow-Band Formation and Evolution During the 15 November 1987 Aircraft Accident at Denver Airport. *Weather and Forecasting*, Vol. 3, No. 4, p453.

Rauber, R.M., and L.O. Grant, 1985: COSE IV Operation Log. Department of Atmospheric Science, Colorado State University, Fort Collins CO. 183 pp.

Rauber, R.M., L.O. Grant, D. Feng, and J.B. Snider, 1986: The Characteristics and Distribution of Cloud Water over the Mountains of Northern Colorado during Wintertime Storms. Part I: Temporal Variations. *Journal of Climate and Applied Meterology*, Vol. 25, No. 4, 468-488.

Rauber, R.M., and L.O. Grant, 1986: The Characteristics and Distribution of Cloud Water over the Mountains of Northern Colorado during Wintertime Storms. Part II: Spatial Distribution and Microphysical Characteristics. *Journal of Climate and Applied Meteorology*, Vol. 25, No. 4, 489-504.

Rauber, R.M., 1987: Characteristics of Cloud Ice and Precipitation during Wintertime Storms over the Mountains of Northern Colorado. *Journal of Climate and Applied Meteorology*, Vol. 26, No. 4, 488-524.

Rogers, D.C., R.M. Rauber and L.O. Grant, 1986: Final Report to Utah Department of Natural Resources: Studies of Wintertime Storms Over the Tushar Mountains of Utah. *Colorado State University, Department of Atmospheric Science.* Fort Collins, CO. 50 pp.

Reynolds, D.W., and Kuciauskas, A.P., 1988: Remote and In Situ Observations of Sierra Nevada Winter Mountain Clouds: Relationships between Mesoscale Structure, Precipitation and Liquid Water. *Journal of Applied Meteorology*, Vol. 27, No. 2, 140-156.

Sassen, K., 1984: Deep Orographic Cloud Structure and Composition Derived from Comprehensive Remote Sensing Instruments. *Journal of Climate and Applied Meteorology*, Vol. 23, No. 4, 568-583.

Sassen, K. 1987: Ice Cloud Content from Radar Reflectivity. *Journal of Climate and Applied Meteorology*, Vol. 26, August 1987, 1050-1053.

Sassen, K., A.W. Huggins, A.B. Long, J.B. Snider and R.J. Meitín, 1990: Investigations of a Winter Mountain Storm in Utah, Part II: Mesoscale Structure, Supercooled Liquid Water Development, and Precipitation Processes. *Journal of the Atmospheric Sciences*, Vol. 47, No. 11, 1323-1350.

Sato, N., K. Kikuchi, S.C. Bernard, and A.W. Hogan, 1981: Some Characteristic Properties of Ice Crystal Precipitation in the Summer Season at South Pole Station, Antarctica. *Journal of the Meteorological Society of Japan*, Vol. 59, No. 5, 772-780.

Seigal, A.D., 1977: Oceanic Latent and Sensible Heat Flux Variability and Air-Interaction. *Colorado State University, Environmental Research Paper No. 7*, 31 pp.

Uttal T., R.M. Rauber, and L.O. Grant, 1988: Distributions of Liquid, Vapor, and Ice in an Orographic Cloud from Field Observations. *Journal of the Atmospheric Sciences*, Vol. 45, No. 7, 1110-1122.

Vali, G., M.K. Politovich and D.G. Baumgardner, 1981: Conduct of Cloud Spectra Measurements. Final Report AFGL-TR-81-0122, Department of Atmospheric Science, University of Wyoming, 69 pp.

Wexler, R., 1954: Radar Analysis of Precipitation Streamers Observed 25 February 1954. *Journal of Meteorology*, Vol. 12, August 1955, 391-393.

Wexler, R. and D. Atlas, 1959: Precipitation Generating Cells. *Journal of Meteorology*, Vol. 16, June 1959, 327-332.